

CLASSIFICATION CHANGE

To *Unclassified*  
By authority of *NASA Memo dtd 5-2-73/SL by H. Maines*  
Changed by *M. Ruda* Date *6-7-77*

**NACA**

# RESEARCH MEMORANDUM

INVESTIGATION IN SIMULATED VERTICAL DESCENT OF THE  
CHARACTERISTICS OF A CARGO-DROPPING DEVICE

HAVING EXTENSIBLE ROTATING BLADES

By Ralph W. Stone, Jr., and Burton E. Hultz

Langley Aeronautical Laboratory  
Langley Air Force Base, Va.

*REVIEW COPY*

THIS MATERIAL CONTAINS INFORMATION AFFECTING THE  
NATIONAL DEFENSE OF THE UNITED STATES WITHIN THE  
MEANING OF THE Espionage Laws, TITLE 18, U. S. C.  
OF WHICH IN ANY MANNER TO DISCLOSE OR  
IS PROHIBITED BY LAW.

Restriction/Classification Cancelled

**NATIONAL ADVISORY COMMITTEE  
FOR AERONAUTICS  
WASHINGTON**

**FILE COPY**  
to be returned to  
the files of the National  
Advisory Committee  
for Aeronautics  
Washington, D. C.

July 1949

~~SECRET~~

NATIONAL ADVISORY COMMITTEE FOR AERONAUTICS

---

SPECIAL REPORT

---

INVESTIGATION IN SIMULATED VERTICAL DESCENT OF THE  
CHARACTERISTICS OF A CARGO-DROPPING DEVICE  
HAVING EXTENSIBLE ROTATING BLADES

By Ralph W. Stone, Jr., and Burton E. Hultz

SUMMARY

An investigation of the characteristics of a cargo-dropping device with extensible rotating blades as load-carrying surfaces in simulated vertical descent has been conducted in the Langley 20-foot free-spinning tunnel. The results of the investigation indicated that a device having rotating airfoil blades restrained centripetally by extensible cables could be made to support weight in steady vertical descent and that proper functioning would depend on accurate dynamic mass balancing of the blades. It was also indicated that it is possible to make such a device so that, when it is exposed to an air velocity along its axis of rotation with the cables retracted and the blades stationary, the blades will accelerate in rotation and will extend the cables smoothly against a spring load until the blades are rotating steadily at the limit of the cable extension.

INTRODUCTION

In accordance with a request made of the National Advisory Committee for Aeronautics, an investigation was performed in the Langley 20-foot free-spinning tunnel to determine the characteristics of a  $\frac{1}{4}$ -scale model of a cargo-dropping device for determining the practicability of such a device. This device utilizes four extensible rotating blades as load-carrying surfaces. The blades, which are mounted by steel cables to a spring-loaded drum mounted above a cylindrical cargo container, extend when their rotational speed is sufficiently large and fly in a circular path at a large radius. It was estimated by the designers, who were present during the investigation, that the device could be dropped at an indicated airspeed

~~SECRET~~

of 300 miles per hour at 30,000 feet altitude with a 2000-pound load and that it would have a sinking velocity just prior to contact with the ground of 60 to 70 feet per second. *44 mph*

## SYMBOLS AND COEFFICIENTS

b	span of blade, feet
$\bar{c}$	mean aerodynamic chord of blade, feet
c	local chord of blade, feet
S	area of blade, square feet
R	radius of rotation of any given point on blade, feet
$R_m$	distance from center of rotation to point along blade span which has average dynamic pressure, feet
m	mass of blade
$x/\bar{c}$	ratio of distance between center of gravity and leading edge of mean aerodynamic chord to mean aerodynamic chord of each blade
$I_{XB}, I_{YB}, I_{ZB}$	moments of inertia of each blade about X, Y, and Z body axes of blade, respectively
$\delta_t$	tab setting, degrees
n	number of blades
W	weight of entire model, pounds
$I_Z$	moment of inertia of entire blade assembly and hub about vertical axis of model
$S_p$	projected area of model, excepting blade, in horizontal plane, square feet
$\alpha$	angle of attack of blade, degrees
$\sigma$	helix angle of blade, angle between flight path and vertical, degrees

$\theta$	angle between chord axis and horizontal, degrees, positive when leading edge of chord is above horizontal
$\phi$	angle between span axis of blade and horizontal, degrees, positive when the tip chord is below the root chord
V	vertical velocity, feet per second
$\Omega$	angular velocity of blade assembly about vertical axis, radians per second
$\rho$	air density, slugs per cubic foot
p	rolling angular velocity, radians per second
q	pitching angular velocity, radians per second
r	yawing angular velocity, radians per second
L	total lift of blades, pounds
D	total drag of blades and attaching cables, pounds
$D_p$	drag of entire model excepting blades, pounds
$C_L$	lift coefficient of each blade $\frac{L/n}{\frac{1}{2} \rho (V^2 + \Omega^2 R_m^2) S}$
$C_D$	drag coefficient of each blade including component of drag of attaching cable $\frac{D/n}{\frac{1}{2} \rho (V^2 + \Omega^2 R_m^2) S}$
$C_{Dp}$	drag coefficient of entire model excepting blades including component of drag of attaching cables $\left( \frac{D_p}{\frac{1}{2} \rho V^2 S_p} \right)$
t	time, seconds
$L'$	rolling moment, foot-pounds
M	pitching moment, foot-pounds

$N$	yawing moment, foot-pounds
$\rho_B$	density of blade material, slugs per cubic foot
$C_{Lr}$	rate of change of rolling-moment coefficient with $\frac{rb}{2\sqrt{\Omega^2 R_m^2 + v^2}}$ , $\left(\frac{\partial C_L}{\partial \left(\frac{rb}{2\sqrt{\Omega^2 R_m^2 + v^2}}\right)}\right)$
$C_{Nr}$	rate of change of yawing-moment coefficient with $\frac{rb}{2\sqrt{\Omega^2 R_m^2 + v^2}}$ , $\left(\frac{\partial C_N}{\partial \left(\frac{rb}{2\sqrt{\Omega^2 R_m^2 + v^2}}\right)}\right)$
$K_1$	$\left(n \frac{\rho}{2} S\right)$
$K_2$	$\left(C_{Dp} \frac{\rho}{2} S_p\right)$

## Subscripts:

1	inboard tip of blade
2	outboard tip of blade
cg	center of gravity of blade

## APPARATUS AND METHODS

## Model

The  $\frac{1}{4}$ -scale model of the cargo-dropping device was furnished by the Pioneer Electric and Research Company who designed the device with Mr. Ward Beman acting as consultant. A drawing of the general arrangement of the model in its original design condition is shown in figure 1, and a detailed drawing of a blade is shown in figure 2. The blades had an NACA 65A012 airfoil section. As shown in figure 1, the blades were mounted on a spring-loaded drum on top of the cylindrical load-carrying body. The blades were attached to the spring-loaded drum by aircraft cables which attached to the blades as shown in figure 2 and were coiled about the drum; the cables were carried from the blade center section to the inner tip internally along the blade spar. When rotating, the centrifugal force of the blades tended to uncoil the cables from the drum. This effect was resisted by a spring which exerted approximately 5 pounds of centripetal force on each blade with the cables fully

retracted and approximately 20 pounds on each blade with the cables fully extended. Each model blade unit weighed about 50 grams. Each blade was originally balanced to have its center of gravity at the cable attachment. When fully extended, the tip radius of the model was 6 feet. As shown in figure 2, each blade had a tab installed and provisions were made for testing the model with a tab-setting range of  $\pm 25^\circ$ . The cylindrical cargo container had vanes installed on its periphery which caused the body to rotate independently of the blade system and in the opposite direction.

The basic principle of operation of the device is that as the unit is dropped, air flow over the blades imparts a rotating motion to the blade assembly. As the rate of rotation increases with increased vertical velocity, the centrifugal force of the blades acts against the spring-loaded cable and causes the blades to extend. When fully extended, the blades have a large radius and a high rate of rotation and therefore a large airspeed relative to the rate of vertical descent of the device. Thus it is expected that a relatively large lift will be produced by the small blades (depending on their tab settings) and a relatively slow and well-stabilized descent will be obtained. It was indicated by the designers that on the full-scale device the blades would be trimmed to operate at a lift coefficient of approximately 0.65 and that their tip speed would be limited by the blade drag characteristics to a Mach number of about 0.7.

#### Wind Tunnel and Testing Technique

The model was tested in the Langley 20-foot free-spinning tunnel, the operation of which is generally similar to that described in reference 1. For these tests, however, the model was mounted by cables in the center of the tunnel as shown on figure 3. The model was suspended freely from the top by a cable attached to a weight pan and weights. A cable was attached to the bottom of the model and anchored to the floor. The tests were performed with slack in the lower cable so that it had little or no influence on the model performance. This was possible because, during the tests, the aerodynamic lift of the model did not exceed the weight of the model and the suspension system. The suspension system was so arranged that the slack in the lower cable could be removed to restrain the model in an emergency. Guy wires above and below the model restricted lateral motion of the model. Free-turning bearings at the cable connections of the model allowed the model to rotate freely.

In the tunnel, the vertical descent of the model was simulated by the vertically rising air stream. The rate of rotation of the model was measured by use of a strobotac. Motion pictures were taken of the rotating blades during the test. The lift of the model was measured by adjusting the weights on the upper cable and sustaining the model at

a fixed height in the tunnel. Tests were also performed on the blade to measure the variation of the angle of attack of the blade with a variation of tab setting. These tests were performed with the equipment shown in figure 4. The blade was mounted on a pivot rod placed within the hollow spar in which the attaching cable is normally located. The blade was also restrained from vibrations by a fine wire normal to the blade, spanning a yoke between which the blade was mounted. The measuring device was extended into the vertically rising air stream with the blade span horizontal thus allowing the blade to pivot longitudinally about the pivot rod to its trim angle of attack. The angles of attack were recorded for each of several tab settings.

### TESTS

The test program and the model configuration for each of the tests are presented in table I. Remarks on the model behavior for each test are also presented in table I. The results of measurements of the rate of rotation and of the lift force are presented in table II. Figure 5 presents the measured variation of blade trim angle of attack with tab deflection.

### RESULTS AND DISCUSSION

Prior to the tests in the Langley 20-foot free-spinning tunnel, preliminary tests had been performed by the designers on a rotary-wing blade assembly. The blade assembly tested was similar to that shown in figure 1 except the blades did not have the taper or the sweptback outer panel of the present configuration (fig. 2). The tests consisted of driving the blade assembly by a motor so that the blades extended and flew at their full radius. Vertical descent, however, was not simulated and therefore, although there was a variation of dynamic pressure spanwise along the blade, there was not a variation in angle of attack as there would be in the actual case of vertical descent. Also, these preliminary tests did not establish that autorotation of the blade system could be started by an initial velocity perpendicular to the plane of rotation of the blades.

Tests were therefore performed in the Langley 20-foot free-spinning tunnel to determine the effects of the vertical velocity component on the characteristics of the device. An analysis of the forces and moments acting on the autorotating blades in vertical descent is given in the appendix. Derivations of equations of some of the forces and moments are also included in the appendix.

The model was first tested in its original configuration without the cargo container or its vanes installed. Tests 1 to 4 (table I) were performed with the model in this basic configuration with the blade tabs set at  $-5^{\circ}$ , at  $0^{\circ}$ , and with tabs removed. For these tests, flapping oscillations started at a very low airspeed and before the blades extended from the hub of the rotor system. Study of motion-picture film of the motion shows that pitching oscillations were also existent. The oscillations were so violent and large in magnitude that the test was stopped and the configuration was considered unsatisfactory. It was at first felt that this unsatisfactory condition may have resulted because of the initial high angle of attack on the blade at starting. With the blades set horizontally ( $\theta = 0^{\circ}$ ), the initial angle of attack was  $90^{\circ}$  to the vertical air stream. The blades tended to remain at this high angle of attack, and it was thought that the aerodynamic pitching moment of the blades may be such that two trim points may exist, one below and one above the stall. A test was therefore performed in which the initial settings of the blades were varied from their original positions until they were about  $10^{\circ}$  from the vertical ( $\theta = 80^{\circ}$ ); when the vertical air flow started, however, the blades trimmed to  $\theta = 0^{\circ}$  and behaved as previously discussed.

It appeared that the blades were longitudinally unstable and tests were therefore performed with the center of gravity of each blade moved forward 8 percent  $\bar{c}$ . This was done by adding weight to the blades ahead of their mounting point. The tests performed for this configuration (tests 5, 6, and 7, table I) resulted in performance of the device similar to the results for the original center-of-gravity position. It was apparent from these tests that something other than the static longitudinal aerodynamic stability of the blades was causing their erratic behavior.

In order to facilitate testing, two of the four blades were removed from the model. It was felt that the results with two blades would be an adequate indication of the performance of the model, and the remainder of the investigation was performed with only two blades. At first, weights were attached to the cables of the two blades which had been removed. Subsequently during the test program, when a method of satisfactorily extending the blades was found, these weights were reduced in size and eventually the weights and cables were removed altogether. The only influence of these changes appeared to be a variation in the rate of rotation at which the blades started to extend from the hub.

It was felt that the blade oscillations obtained may have resulted because of stalling of the blades associated with the extreme variation in angle of attack when the blades were retracted (analysis presented in appendix). In order to alleviate this possible condition of stalling, cuffs were installed on the hub into which the blades fitted (fig. 6).

The cuffs were so arranged that the part of the blades extending beyond the cuffs would be below the stall when the rate of rotation of the blades was sufficient for the blades to extend. The parts of the blades enclosed in the cuffs, which would normally be stalled, were shielded from the air stream and therefore had no influence on the aerodynamic characteristics of the blade.

Tests 8, 9, and 10 were performed for this condition of the model with the cargo container removed. Tab settings of  $\pm 10^\circ$  were used for the tests. For all tests, the blades moved out of the cuffs satisfactorily but when the blades were finally free of the cuffs, they became violently oscillatory in flapping and pitching as for the previous tests. A film strip showing the motion of the blades after they had extended from the cuffs is presented in figure 7.

After practical consideration had been given to the primary aerodynamic problems, static longitudinal stability and the stall, because unsatisfactory characteristics were still obtained, consideration was next given to the inertia moments acting on the blades. An analysis of the inertia moments acting on the blades is included in the appendix. Analysis indicated that if the inertia pitching moment was larger than the aerodynamic nose-down pitching moment, the blades would tend to trim at  $\theta = 0^\circ$ . If such were true, the blades would stall and thus cause the troubles encountered so far. It would appear therefore that, if  $I_{XB}$  equalled  $I_{ZB}$ , no inertia pitching moment would exist. The moment of inertia  $I_{ZB}$  of the blade was estimated to be somewhat larger than  $I_{XB}$  and, therefore, in order to increase  $I_{XB}$  to equal  $I_{ZB}$ , weight was added along the Z-axis. In addition to changing the inertia moments, the center of gravity was also moved forward 4 percent  $\bar{c}$  so as to increase the aerodynamic longitudinal stability and also to compensate for a yawing moment about the blade-attachment point resulting from centrifugal forces acting on the sweptback blade. An analysis of this yawing moment is given in the appendix. Figure 8 is a sketch showing how weight was added to the blade. Tests 11 to 18 were performed with the blades so modified. Figure 9 is a photograph of the model in this condition. In test 11, oscillations were still obtained and it was decided that insufficient weight had been added along the Z-axis so larger weights were installed. Tests 12 and 13 proved successful in that the blades extended and flew well. After the blades had fully extended and the airspeed had been increased, however, an oscillation developed in the vertical supporting portion of the body. The lower end of the vertical portion of the body tended to move out from the vertical axis and move in a circular arc in the same direction as the rotation of the device. It was felt that this effect may have been the result of gyroscopic moments which might have

been aggravated because the rotation rates were equal to or harmonics of the natural frequency of the suspension system.

In order to reduce the oscillations of the vertical portion of the model, it was felt that installation of the load-carrying body with its vanes (which cause a counterrotation of the body) would cause a gyroscopic moment in opposition to the gyroscopic moment of the rotating blade system. A photograph of the model with the body installed is shown in figure 10.

Test 14 was performed in this condition and the model operated satisfactorily. A film strip showing the blades flying in their fully extended condition is presented in figure 11. Because of the limited view of the camera, only one blade can be seen in any given frame and also because of the high rate of rotation relative to the camera speed (64 frames per second) the blades can only be seen as blurs. Small oscillations of the vertical axis of the body and a precessional motion of the entire device, however, were still observed. Variation of tension in the supporting cables was found to cause an aggravation or alleviation of this motion. It was possible, by adjusting the tension, to obtain rotational speeds of the blades which were beyond a critical range for which the oscillations existed. From these tests, it would appear that the oscillation of the vertical body was primarily an inherent part of the suspension system and that, in free descent, such troubles might not be encountered. It is felt, however, that further consideration of such gyroscopic moments should be given in the final design. A series of measurements of vertical velocity and rotational velocity were made, as listed in table II. At the highest rotational velocity reached, one of the cuffs failed and seriously damaged one blade.

Because the blades had performed satisfactorily after adequate alteration of the inertia pitching moment, it was felt that the cuffs could now be removed. Tests 15 to 18 were performed with the cuffs removed from the model for different tab settings. For these tests, the blades extended in a satisfactory manner; but as the airspeed was increased after full extension, the blades seemed to hesitate in rotation, the rotation decreased, and the blades started to retract toward the hubs. After partially retracting, the rotation steadied out and the blades extended fully, until the procedure repeated itself. Reduction of the tab setting tended to reduce this effect and the motion was sufficiently steady with zero tab setting to obtain some numerical data (test 18, tables I and II). The hesitation in rotation or the dragging of the blades still occurred, however, and the configuration was not considered completely satisfactory.

Inasmuch as during the tests with cuffs installed, the model did not have this particular undesirable motion, it appeared that they prevented this motion and cuffs were therefore reinstalled. Test 19 (the final test of the program) with cuffs installed proved entirely successful. An explanation of the actual effects of the cuffs in preventing the motion is not available; it appears, however, that cuffs should be used until a better method of preventing the motion is available.

As previously indicated, the investigation of the performance was primarily limited to the results of test 19 (tables I and II). For this test, a tab deflection of  $-12^\circ$  was arbitrarily used. The variation of the vertical force with vertical velocity for this test is presented in table II and plotted in figure 12. Also shown in figure 12 is a plot of a theoretical variation of vertical force with vertical velocity computed on the basis of the theoretical variation of vertical velocity with weight as presented in the appendix. The results of figure 12 show good agreement between the experimental and theoretical values for this tab setting. The experimental values of vertical rate of descent for any given loading, however, were somewhat smaller than those estimated theoretically. From the trend of the curves, it appears that beyond the maximum velocity tested the experimental velocity would have been somewhat larger than that calculated. In order to compensate for these slight differences, an empirical correction was applied to the theoretical calculations. Theoretical values so corrected are also shown on figure 12. The slight discrepancy between experiment and theory may have been, in part, the result of the fact that although the theoretical calculations are based on a constant value of  $L/D$ , the corresponding experimental measurements of table II indicate a slight variation in this ratio. This variation may be the result of slight changes in trim of the blades possibly caused by unbalanced centrifugal or inertia moments on the blades and/or changes in the aerodynamic characteristics of the blade because of compressibility effects (neglected in the computations).

The calculations were made by the use of equation (10) developed in the appendix. The lift- and drag-coefficient data used for the calculations were obtained from reference 2 for an NACA 65<sub>1</sub>-012 airfoil section. The actual airfoil section of the model, NACA 65A012, is an NACA 65<sub>1</sub>-012 section with the cusp removed, and it is believed that the differences in the sections would not greatly affect the aerodynamic coefficient data used for the computations. The values of  $C_D$  used in the calculations included not only the effects of the blade and an estimated component of cable drag acting on the blade but also a small estimated increment due to the compensating weights mounted on the blades. The estimated increment of drag coefficient of the compensating weights was not varied for the effects of angle of attack in that the

increment was a relatively small proportion of the over-all drag. The lift data were corrected for the effects of aspect ratio. Estimations of the effect of tab settings were applied to both the lift- and drag-coefficient data by the methods of reference 3. These estimations of the lift- and drag-coefficient data for a blade are presented in figure 13 for tab settings of  $-5^{\circ}$ ,  $-10^{\circ}$ ,  $-12^{\circ}$ ,  $-15^{\circ}$ , and  $-20^{\circ}$ . The trim angles of attack of the blades used for the calculations which were obtained experimentally were obtained from figure 5. The actual measurements on figure 5 show a negative angle of attack of  $3^{\circ}$  for zero tab setting; but since the blade section is symmetrical and should have an angle of attack of  $0^{\circ}$  for zero tab setting, it was felt that this effect was the result of interference of the measuring equipment (fig. 4) and the curve was shifted to the origin for use in all calculations herein.

The contribution to the vertical force of the drag of the cargo container and appendages was determined by estimating a value of  $C_{D_p}$  from existing information on the drag of cylinders and cables. A component of drag of the attaching cables was included in  $C_{D_p}$ . A value of  $C_{D_p}$  of 1.10, based on the horizontally projected area of the cargo container, was used in the computations.

#### Estimated Performance of Full-Scale Device

Estimations were made of the probable performance of the full-scale cargo-dropping device with four blades installed. The effects of variations in tab setting and in altitude on the vertical-descent characteristics of the device were determined by consideration of the force equation (equation (10) of appendix). The estimated aerodynamic data of figure 13 for different tab settings were used, and the small empirical correction previously mentioned was applied.

Effects of tab settings.— Calculations showing the variation with loading of vertical rate of descent at sea level for several tab settings are presented in figure 14. The results of the theoretical calculations indicate that a 2000-pound load would have a sinking velocity just prior to striking the ground (at sea level) of approximately 45, 59, 78, and 112 feet per second for tab settings of  $-20^{\circ}$ ,  $-15^{\circ}$ ,  $-12^{\circ}$ , and  $-10^{\circ}$ , respectively. A value of sinking velocity of from 60 to 70 feet per second for a 2000-pound load (previously indicated as having been estimated by the designer) could therefore be obtained by use of a tab setting of the order of  $-15^{\circ}$ . The approximate average lift coefficient estimated for the blade for a tab setting of  $-15^{\circ}$  was 0.41. This lift coefficient value is smaller than the value of 0.65 which was estimated by the designers to correspond

with the sinking velocity previously noted. Calculations indicate that with a lift coefficient of 0.65 a sinking velocity of the order of 40 feet per second may be obtained.

Also presented in figure 14 is a curve intersecting the plots of vertical force against vertical velocity for each tab setting at a value of vertical velocity at which the resultant velocity of the blade tip is 0.7 Mach number, which as previously indicated, was the maximum tip speed of the device expected by the designer. In order to determine the extent to which the calculations may be considered adequate, a study of the critical Mach numbers of the blade for the various tab settings was made. A second curve intersecting the plots of vertical force against vertical velocity is included in figure 14. This curve intersects the various plots at a value of vertical velocity at which for each tab setting the resultant velocity of the blade at the radius point  $R_m$  is at critical Mach number. The radius point  $R_m$  was used because it was assumed that the average value of  $C_L$  for the blade would exist at the blade section, a distance of  $R_m$  from the center of rotation. It was also felt that, because of the nature of the variation in angle of attack and airspeed along the blade span, critical Mach number may be encountered along the entire span nearly at once. The plots have been dotted above the critical Mach number curve. The critical Mach numbers were obtained from reference 2. It appears from the plots of figure 14 that the calculation gives an adequate indication of the sinking velocities at sea level for loadings of the order of 2000 pounds or less. If heavier loads are contemplated, consideration of compressibility effects would be necessary for an accurate indication of the sinking velocity.

Effects of altitude.— Computations were made to determine the rate of descent of the device at different altitudes for an arbitrary load of 2000 pounds. The rates of descent at sea level were obtained from figure 14 for each tab setting. For each tab setting, changes in rate of descent were calculated with a variation in altitude on the basis of constant dynamic pressure. These calculations are presented in figure 15. In this figure, as in figure 14, curves intersecting the plots for each tab setting at the limiting Mach number 0.7 and at the critical Mach number are also presented. The variation of the speed of sound with altitude was considered. The plots of vertical velocity against altitude are dotted above the values of critical Mach number, as in the case for figure 14, in that no corrections have been applied for compressibility effects.

Study of figure 15 indicates that at 30,000 feet altitude, a proposed altitude for cargo release, a Mach number of 0.7 may be encountered at the blade tips unless a tab setting of the order of  $-20^\circ$  is used. The release, however, will probably be made at a

forward speed of the order of 300 miles per hour, which generally is in excess of the terminal velocity of the device for any tab setting. The blades therefore will extend at speeds which will tend to cause a blade-tip speed in excess of Mach number 0.7. The effects of the blade-drag rise due to compressibility will therefore influence the path of motion of the device from its release speed to a condition of vertical descent and its terminal velocity as presented on figure 15. Actual calculations of the motion after release with an initial horizontal velocity in excess of the terminal velocity of the device would require measurements of the aerodynamic characteristics of the blades throughout the critical Mach number range.

#### CONCLUDING REMARKS

The results of the investigation indicated that a device having rotating airfoil blades restrained centripetally by extensible cables could be made to support weight in steady vertical descent and that proper functioning would depend on accurate dynamic mass balancing of the blades. It was also indicated that it is possible to make such a device so that, when it is exposed to an air velocity along its axis of rotation with the cables retracted and the blades stationary, the blades will accelerate in rotation and will extend the cables smoothly against a spring load until the blades are rotating steadily at the limit of the cable extension.

Langley Aeronautical Laboratory  
National Advisory Committee for Aeronautics  
Langley Air Force Base, Va.

*Ralph W. Stone, Jr.* per BC7  
Ralph W. Stone, Jr.

Aeronautical Research Scientist

*Burton E. Hultz*  
Burton E. Hultz  
Aeronautical Engineer

Approved:

*Charles N. Zimmerman*

for Thomas A. Harris  
Chief of Stability Research Division

MCF

## APPENDIX

ANALYSIS OF MOMENTS AND FORCES ACTING ON ROTATING BLADES OF  
CARGO-DROPPING DEVICE

A study of the cargo-dropping device primarily involves a study of the aerodynamic characteristics of the blades and how these characteristics of the blades are affected by the curved paths in which the blades are operating.

The angle of attack of the rotating blade is determined, as shown in figure 16, by the following formula:

$$\alpha = 90 - \sigma + \theta \quad (1)$$

where

$$\sigma = \tan^{-1} \frac{\Omega R}{V}$$

Because of a variation in radius from the inner to outer tips, there will be a variation in angle of attack along the blade. The increment in the angle of attack from inner to outer tip would be

$$\Delta\alpha = \alpha_1 - \alpha_2 = \tan^{-1} \frac{\Omega R_1}{V} - \tan^{-1} \frac{\Omega R_2}{V} \quad (2)$$

For the initial condition of starting, the inner ends of the blades are against the hub and they therefore have a very small radius of rotation, 0.396 feet (model value). The outboard ends of the blades for this condition have a radius of 1.729 feet. Because of this variation of radius, the angle of attack would vary appreciably along the span. For the case with the blades fully extended, the outer tip radius is 6 feet and inner tip radius is  $4\frac{2}{3}$  feet. It can be seen therefore that the variation in angle of attack along the blade for the starting condition, with the inner tip of the blade at the hub, would be much larger than for the fully extended condition, and therefore much more critical as regards operation of the device in that condition.

On the rotating blade the forces in the horizontal plane must be in equilibrium so that from figure 16 it can be seen that the horizontal component of lift must equal the horizontal component of drag, plus an inertia force if the blades are accelerating. Thus,

$$L \cos \sigma - D \sin \sigma - \frac{I_Z \frac{d\Omega}{dt}}{R_m} = 0 \quad (3)$$

For the equilibrium case, when  $\Omega$  is constant

$$L \cos \sigma - D \sin \sigma = 0$$

and

$$\frac{L}{D} = \frac{\sin \sigma}{\cos \sigma} = \tan \sigma = \frac{\Omega R_m}{V} = \frac{C_L}{C_D} \quad (4)$$

It appears therefore that, for the case of equilibrium, the variation of  $\Omega R_m$  with  $V$  is proportional to the  $L/D$  ratio. This equation is based on the assumption that the lift and drag coefficients of the blade at the radius point  $R_m$  are the average values of lift and drag coefficient for the entire blade. The experimental results of test 19, presented in table II and figure 12, for the ratio of  $\frac{\Omega R_m}{V}$  are in good agreement with the ratio of  $L/D$  estimated for this condition, thereby substantiating this assumption. The value of  $C_L$  in the equation is the lift coefficient for the airfoil at an angle of attack of zero pitching moment with the tab deflection considered. The value of  $C_D$  must include both an increment of drag coefficient for the blade and an increment of drag coefficient for a component of drag of the attaching cable, as is indicated in the vector diagram in figure 17. An increment of drag coefficient caused by any other appendages on the blade must also be considered.

A thorough analysis of the starting condition will not be made here because of the complication imposed by stall phenomena of the blades and because, for the general case, the blades would be accelerating until fully extended.

When the blades are fully extended, the rate of rotation would adjust itself to the proper value of  $\frac{\Omega R_m}{V}$  in accordance with the lift and drag characteristics of the blade (equation (4)). The device would

then obtain its terminal velocity, for which the vertical-force component of the device would equal the total weight of the device as follows:

$$\begin{aligned} W &= \frac{L}{\sin \sigma} + D_p \\ &= \sqrt{L^2 + D^2} + D_p \end{aligned} \quad (5)$$

The lift of the cargo-dropping device was developed from the basic lift equation

$$L = C_L \frac{\rho}{2} S V^2 \quad (6)$$

which was modified to allow for rotation by integrating elements of blade lift over the span of the blade as follows:

$$\begin{aligned} dL &= C_L \frac{\rho}{2} n \, dS (\Omega^2 R^2 + V^2) \\ dL &= C_L \frac{\rho}{2} n \int_0^c dc \, dR (\Omega^2 R^2 + V^2) \\ L &= C_L \frac{\rho}{2} n \int_0^c dc \int_{R_1}^{R_2} (\Omega^2 R^2 + V^2) dR \end{aligned}$$

but

$$b \int_0^c dc = S$$

therefore

$$L = n C_L \frac{\rho}{2} S \int_{R_1}^{R_2} \frac{\Omega^2 R^2 + V^2}{b} dR$$

$$L = nC_L \frac{\rho}{2} S \left[ \frac{\Omega^2 R^3}{3b} + \frac{RV^2}{b} \right]_{R_1}^{R_2}$$

For the fully extended condition on the model,  $R_1 = 4.66$  feet and  $R_2 = 6.0$  feet so that

$$L = nC_L \frac{\rho}{2} S \left( \frac{38.09\Omega^2}{b} + \frac{1.33V^2}{b} \right)$$

therefore, since  $b = 1.33$  feet,

$$L = nC_L \frac{\rho}{2} S (28.57\Omega^2 + V^2)$$

In that this integration has led to the average dynamic pressure over the blade,  $R_m^2$  equals  $28.57$  feet<sup>2</sup> and

$$L = nC_L \frac{\rho}{2} S (R_m^2 \Omega^2 + V^2) \quad (7)$$

As has been previously indicated, the derivation assumes that the values of the aerodynamic coefficients of the blade at the mean radius point  $R_m$  are the average aerodynamic coefficients of the entire blade.

The drag of the body can be determined as follows:

$$D_p = C_{D_p} \frac{\rho}{2} S_p V^2 \quad (8)$$

The value of  $C_{D_p}$  includes not only an increment of drag coefficient for the cargo container and its appendages but also an increment of drag coefficient for the component of the drag of the attaching cables parallel to the longitudinal axis of the body as shown in figure 17.

The vertical rate of descent of the device for any given loading could be obtained by consideration of equation (5) and substitution of equations (7) and (8) therein. Equation (5) with these substitutions becomes

$$W = \frac{C_L K_1 (R_m^2 \Omega^2 + V^2)}{\sin \sigma} + K_2 V^2 \quad (9)$$

where

$$K_1 = n \frac{\rho}{2} S$$

and

$$K_2 = C_{Dp} \frac{\rho}{2} S_p$$

since  $R_m \Omega = V \tan \sigma$  (from equation (4)),

$$W = \frac{C_L K_1 (v^2 \tan^2 \sigma + v^2)}{\sin \sigma} + K_2 v^2$$

$$v^2 = \frac{W \sin \sigma}{C_L K_1 (\tan^2 \sigma + 1) + K_2 \sin \sigma}$$

From the geometry of the force vectors acting on the blade (fig. 16) the following substitution is made:

$$\sin \sigma = \frac{C_L}{\sqrt{C_L^2 + C_D^2}}$$

also from equation (4)

$$\tan \sigma = \frac{L}{D} = \frac{C_L}{C_D}$$

therefore

$$v^2 = \frac{W \sqrt{C_L^2 + C_D^2}}{K_1 \left[ \left( \frac{C_L}{C_D} \right)^2 + 1 \right] + K_2 \frac{1}{\sqrt{C_L^2 + C_D^2}}}$$

$$v^2 = \frac{W}{K_1 \sqrt{C_L^2 + C_D^2} \frac{C_L^2 + C_D^2}{C_D^2} + K_2}$$

$$v = \sqrt{\frac{W}{C_D K_1 \left( \frac{C_L^2}{C_D^2} + 1 \right)^{3/2} + K_2}} \quad (10)$$

where

$K_1$  for model with two blades is 0.000702

$K_1$  for full-scale device with four blades is 0.02245

$K_2$  for model is 0.000578

$K_2$  for full-scale device is 0.00925

Other factors which will influence the orientation of the blades, and thus the angle of attack at which the blades are operating, are the inertia moments and centrifugal moments acting on the blades. The inertia moments acting on the blades are as follows:

$$M = (I_{Z_B} - I_{X_B})pr \quad (11)$$

$$N = (I_{X_B} - I_{Y_B})pq \quad (12)$$

$$L' = (I_{Y_B} - I_{Z_B})qr \quad (13)$$

where

$$p = \Omega \sin \theta \cos \phi$$

$$q = \Omega \sin \phi$$

$$r = \Omega \cos \theta \cos \phi$$

and (fig. 18)

$$\phi \approx -\sin^{-1} \frac{L/\sin \sigma}{mR_{cg}\Omega^2}$$

The inertia pitching moment  $M$ , on the blade (where  $I_{Z_B}$  is normally larger than  $I_{X_B}$ ) would be such as to cause the blade to trim in a chordwise horizontal position ( $\theta = 0$ ). The inertia rolling moment (where  $I_{Z_B}$  is normally larger than  $I_{Y_B}$ ) would be such as to cause the blade to trim in a spanwise horizontal position ( $\phi = 0$ ). The inertia yawing moment of the blade (where  $I_{X_B}$  is normally larger than  $I_{Y_B}$ ), will always be a prorotational moment because the angle  $\phi$  is always such as to have the outer tip higher than the inner tip, that is, the moment on the blade about its center of gravity will be in the same direction as the blade is rotating.

Because the blades of the device are mounted flexibly and because the blades have sweep, there is an asymmetrical centrifugal force set up about the center of gravity of the blade. That is, each element of mass outboard of the center of gravity of the blade has a larger radius and therefore a larger centrifugal force than elements of mass on the inboard portion of the blade. Also, because the outboard half of the blade is sweptback, the elements of mass having the larger centrifugal forces are, on the average, farther back on the blade chordwise than the inboard elements, resulting in a moment about the center of gravity of the blade. A derivation of the yawing moment resulting is as follows:

$$dN = \rho_B(R_{cg} + y)\Omega^2 x \, dx \, dy \, dz$$

$$N = \Omega^2 \rho_B \int_{-b/2}^{b/2} \int_{-f(y)}^{f(y)} \int_{-f(x,y)}^{f(x,y)} (R_{cg} + y)x \, dz \, dx \, dy \quad (14)$$

where  $z = f(x,y)$  is a function of the airfoil section,  $x = f(y)$  is a function of the plan-form contours of the blade, and  $\rho_B$  is density of the blade material. If the cable attachment point were at the center of gravity, this moment would augment the previously mentioned inertia yawing moment which caused the blade tip to move forward with relation to blade center of gravity.

The equations used consider only the static aerodynamic characteristics and static and dynamic mass characteristics of the blades. No consideration is given to the effects of the dynamic aerodynamic characteristics such as stability derivatives  $C_{n_r}$  and  $C_{l_r}$  resulting from a yawing velocity  $r$  which the blades undergo when rotating. Nor is consideration given to the friction in the bearing system. The good agreement indicated between theory and experiment, however, indicates that these effects are probably of only minor importance.

## REFERENCES

1. Zimmerman, C. H.: Preliminary Tests in the N.A.C.A. Free-Spinning Wind Tunnel. NACA Rep. 557, 1936.
2. Abbot, Ira H., von Doenhoff, Albert E., and Stivers, Lewis S., Jr.: Summary of Airfoil Data. NACA Rep. 824, 1945.
3. Pearson, H. A.: A Method of Estimating the Aerodynamic Effects of Ordinary and Split Flaps on Airfoils Similar to the Clark Y. NACA TN 571, 1936.

## SECRET

TABLE I.- CONFIGURATIONS TESTED AND OBSERVED RESULTS OF TESTS OF A  $\frac{1}{4}$ -SCALE

MODEL OF A CARGO-DROPPING DEVICE

Test	Number of blades	Load-carrying body and vanes	Counter weights on dummy cables (grams)	Cuffs	Balance weight on blades	Blade center of gravity (percent $\bar{c}$ )	Tab setting, $\delta_t$ (deg)	Initial blade setting, $\theta$ (deg)	Remarks
1	4	Off	----	Off	-----	20	-5	0	Flapping and pitching oscillations, blades did not extend.
2	4	Off	----	Off	-----	20	-5	0	Blades initially set with inner tips 1 inch from hub; flapping and pitching oscillation; blades did not extend.
3	4	Off	----	Off	-----	20	Tabs removed	0	Same as test 1.
4	4	Off	----	Off	-----	20	0	80	Same as test 1.
5	4	Off	----	Off	-----	12	0	80	One blade turned backwards.
6	4	Off	----	Off	-----	12	0	15	Similar to test 1.
7	4	On	----	Off	-----	12	0	15	Same as test 1.
8	2	Off	600	On	-----	20	10	34	Blades extended smoothly until they became disengaged from the cuffs when motion was similar to test 1.
9	2	Off	450	On	-----	20	10	34	Same as test 8.
10	2	Off	450	On	-----	20	-10	34	Same as test 8.
11	2	Off	370	On	Small, on	16	-10	34	Same as test 8.
12	2	Off	370	On	Large, on	16	5	34	Blades extended to full radius and flew smoothly.
13	2	Off	None	On	Large, on	16	-10	34	Blades extended to full radius and flew smoothly; device developed oscillations of vertical body axis.
14	2	On	None	On	Large, on	16	-25	34	Same as test 13; precessing of entire device also took place.
15	2	On	None	Off	Large, on	16	$-17\frac{1}{2}$	0	Guide ring placed below blades when unextended to prevent blades from dropping; damaged blades when rotation started.
16	2	On	None	Off	Large, on	16	$-17\frac{1}{2}$	0	Guide ring removed, blades extended, and device oscillated as in test 13; when sufficient airspeed was obtained, oscillations stopped but blades started a cyclic motion in which the rotation perceptively decreased, the blades started to retract at which time the rotation increased and the blades became fully extended.
17	2	On	None	Off	Large, on	16	-12	0	Same as test 16.
18	2	On	None	Off	Large, on	16	0	0	Same as test 16.
19	2	On	None	On	Large, on	16	-12	34	Blades extended and operated smoothly through a wide range of airspeeds.

<sup>a</sup>Unless otherwise indicated, blades were set initially with inner tips against hub.

SECRET



## SECRET

TABLE II.-- FORCE AND VELOCITY MEASUREMENTS OBTAINED FROM TESTS OF A  $\frac{1}{4}$ -SCALE MODEL OF A

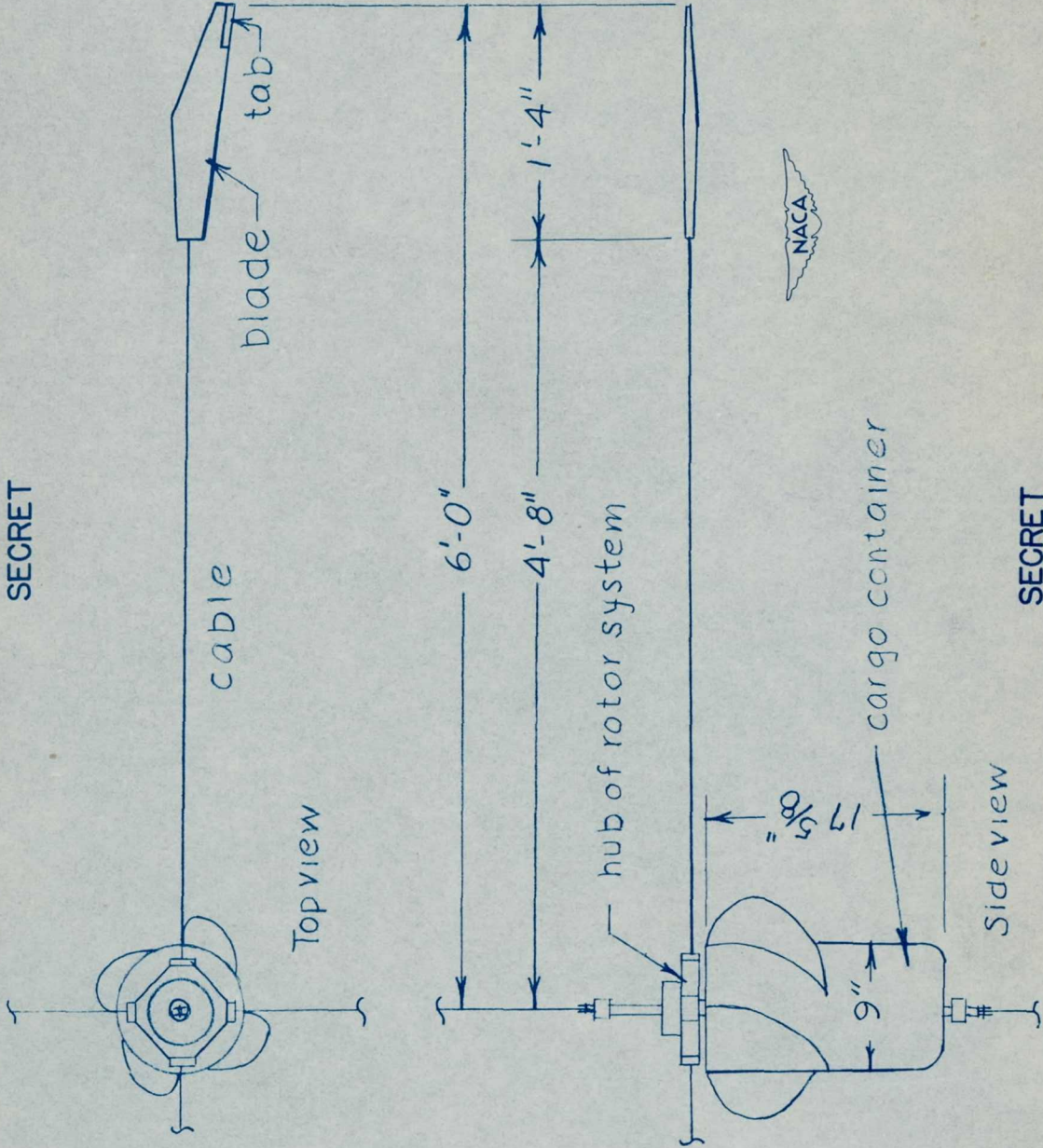
CARGO-DROPPING DEVICE

Test	Operating conditions			Remarks
	Blade rotational speed (rpm)	Tunnel airspeed (ft/sec)	Vertical load (lb)	
1	---	---	---	Rotation started at 15 ft/sec.
2	---	---	---	Rotation started at 15 ft/sec.
3	---	---	---	Rotation started at 12 ft/sec, and blade oscillations started at 350 rpm.
4	---	---	---	Rotation started at 28 ft/sec and blade oscillations started at 300 rpm.
5	---	---	---	---
6	---	---	---	Blade oscillation started at 10.5 ft/sec and 300 rpm.
7	---	---	---	Blade oscillation started at 19 ft/sec.
8	---	---	---	Blade oscillation started at 19 ft/sec when blades disengaged from cuffs.
9	---	---	---	Blade oscillations started at 23 ft/sec when blades disengaged from cuffs.
10	---	---	---	Blade oscillations started at 22 ft/sec when blades disengaged from cuffs.
11	---	---	---	Blade oscillations started at 22 ft/sec when blades disengaged from cuffs.
12	150	33	---	Blades extended at 21 ft/sec.
13	289 350	35.8 40.2	6 9	Blades extended at 30.1 ft/sec, oscillations of vertical body axis started at 42.9 ft/sec.
14	255 300 380 430 445 465	24.6 31.4 38.7 44.3 48.4 52.6	----- ----- ----- ----- ----- -----	Blades extended at 25.9 ft/sec and precessing of body developed; motion restrained by guide cables.
15	---	---	---	---
16	---	---	---	---
17	225 275	25.9 28.7	-----	Values indicate approximate conditions when perceptible decrease in rotation occurred and blades retracted.
18	---	40.2 42.9 54.0 64.0 70.0	----- 4 6 8	Hesitation, as indicated for test 17, occurred at 350 rpm.
19	390 490 525 595 628 660 705	35.0 42.9 46.3 52.6 56.8 61.0 66.2	17.2 23.6 28.1 35.3 39.2 43.3 49.7	---

<sup>a</sup>Conditions existing after blades were fully extended.

SECRET

SECRET



SECRET

Figure 1.— Drawing of  $\frac{1}{4}$ -scale model of cargo-dropping device.

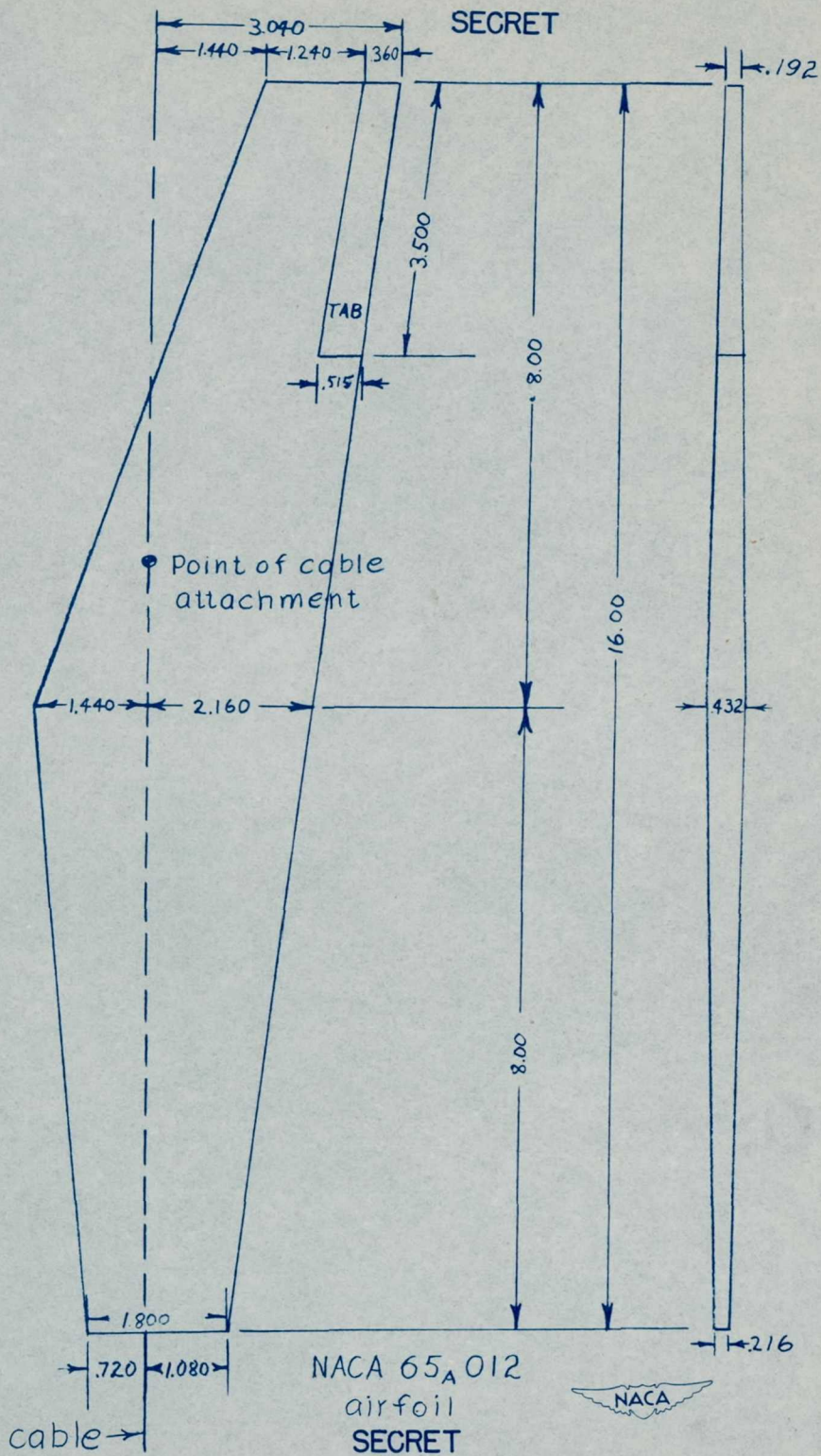
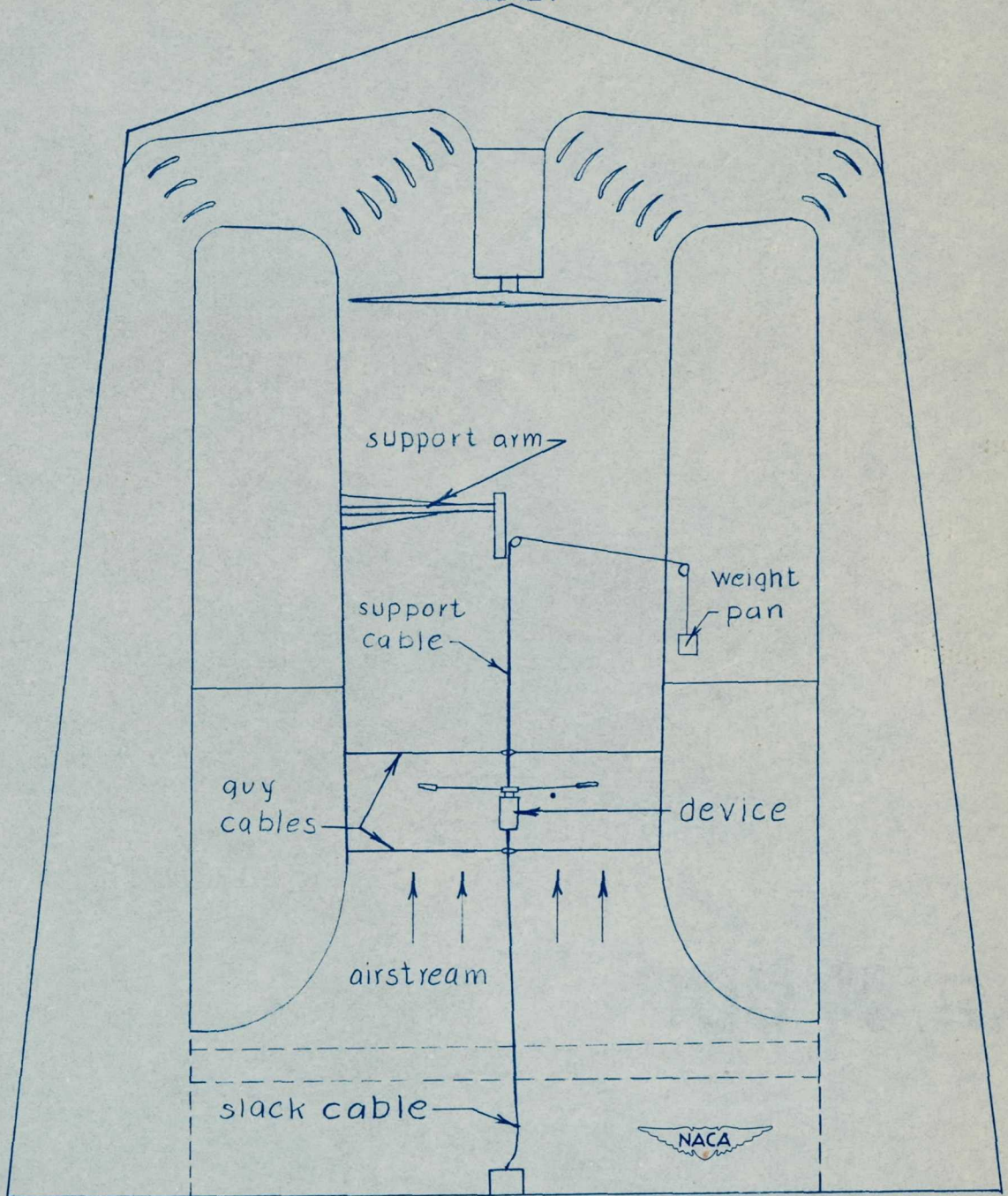


Figure 2.- Blade of  $\frac{1}{4}$ -scale model of cargo-dropping device.

SECRET



SECRET

Figure 3.- One-fourth-scale model of cargo-dropping device mounted in the Langley 20-foot free-spinning tunnel.

SECRET

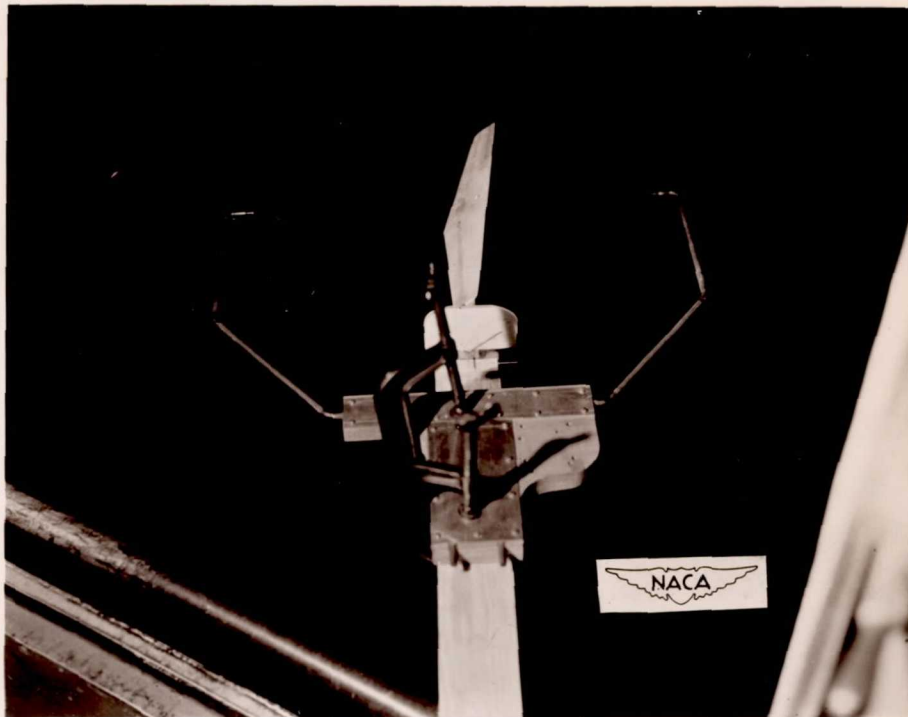


Figure 4.- Device for measuring the variation of trim angles of attack with tab setting.

SECRET

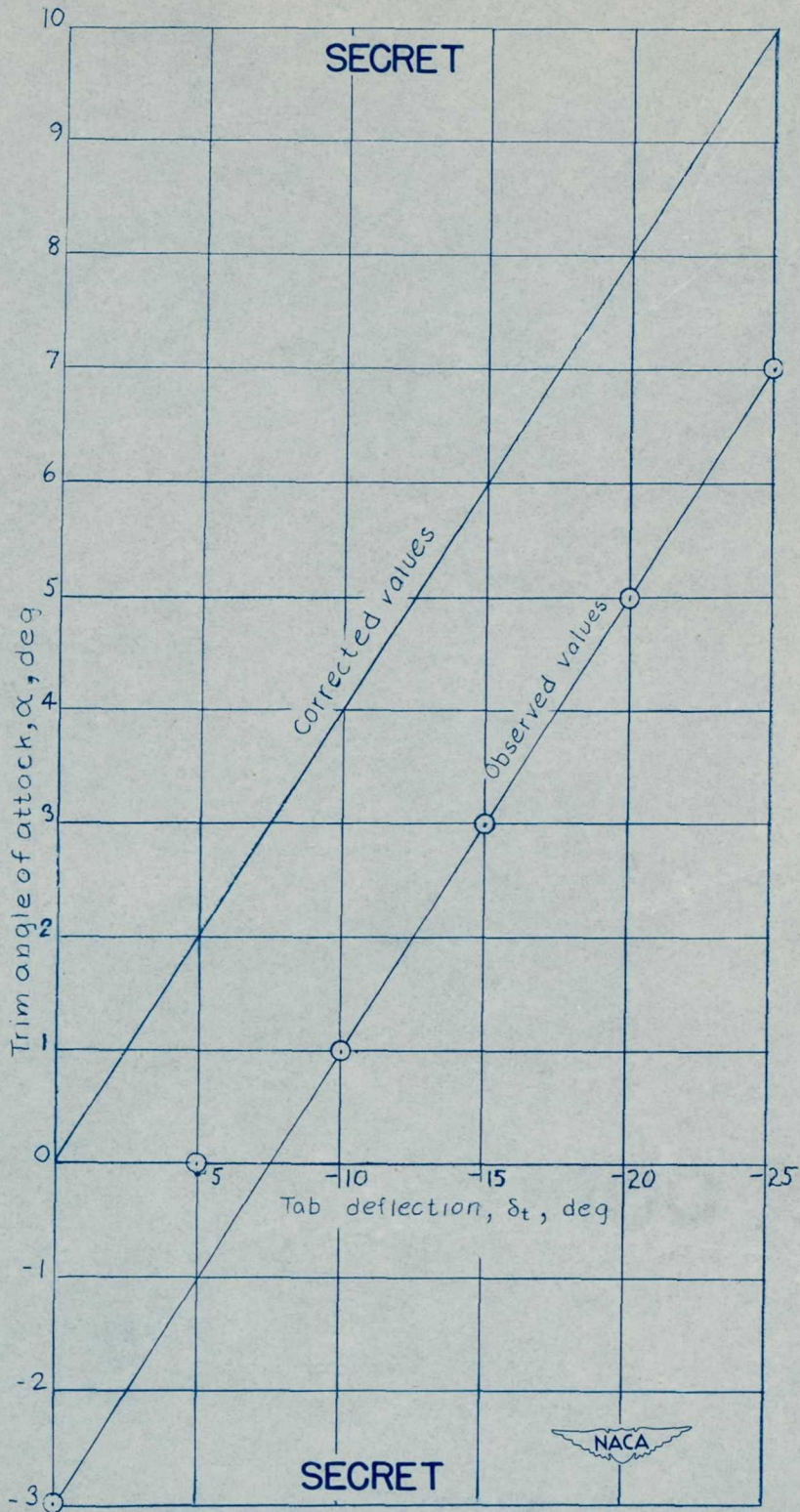


Figure 5.— Trim angle of attack of blade for various tab settings as measured in the Langley 20-foot free-spinning tunnel.

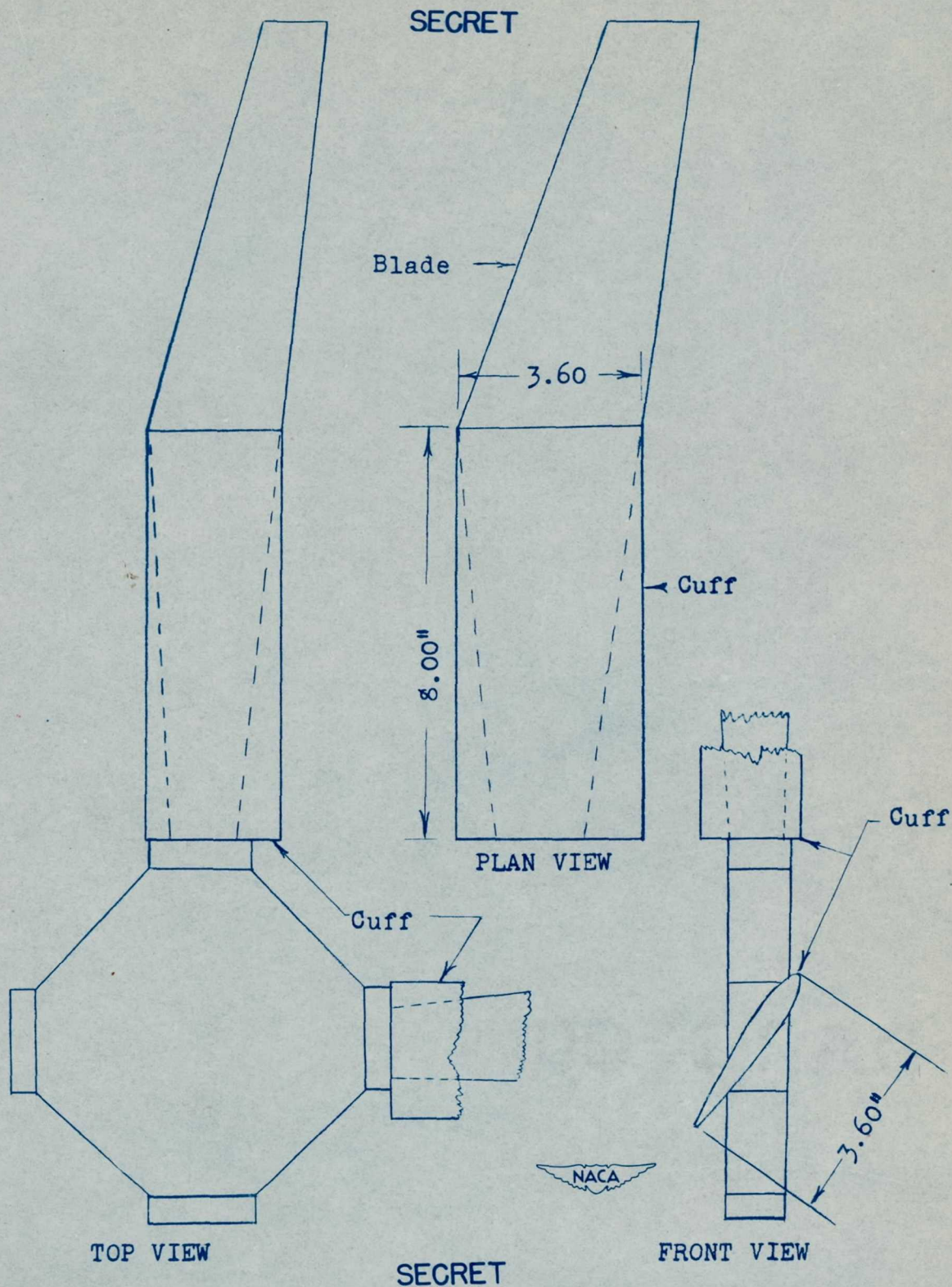


Figure 6.- Cuffs attached to hub of rotor system of  $\frac{1}{4}$ -scale model of cargo-dropping device.

SECRET

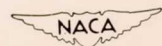
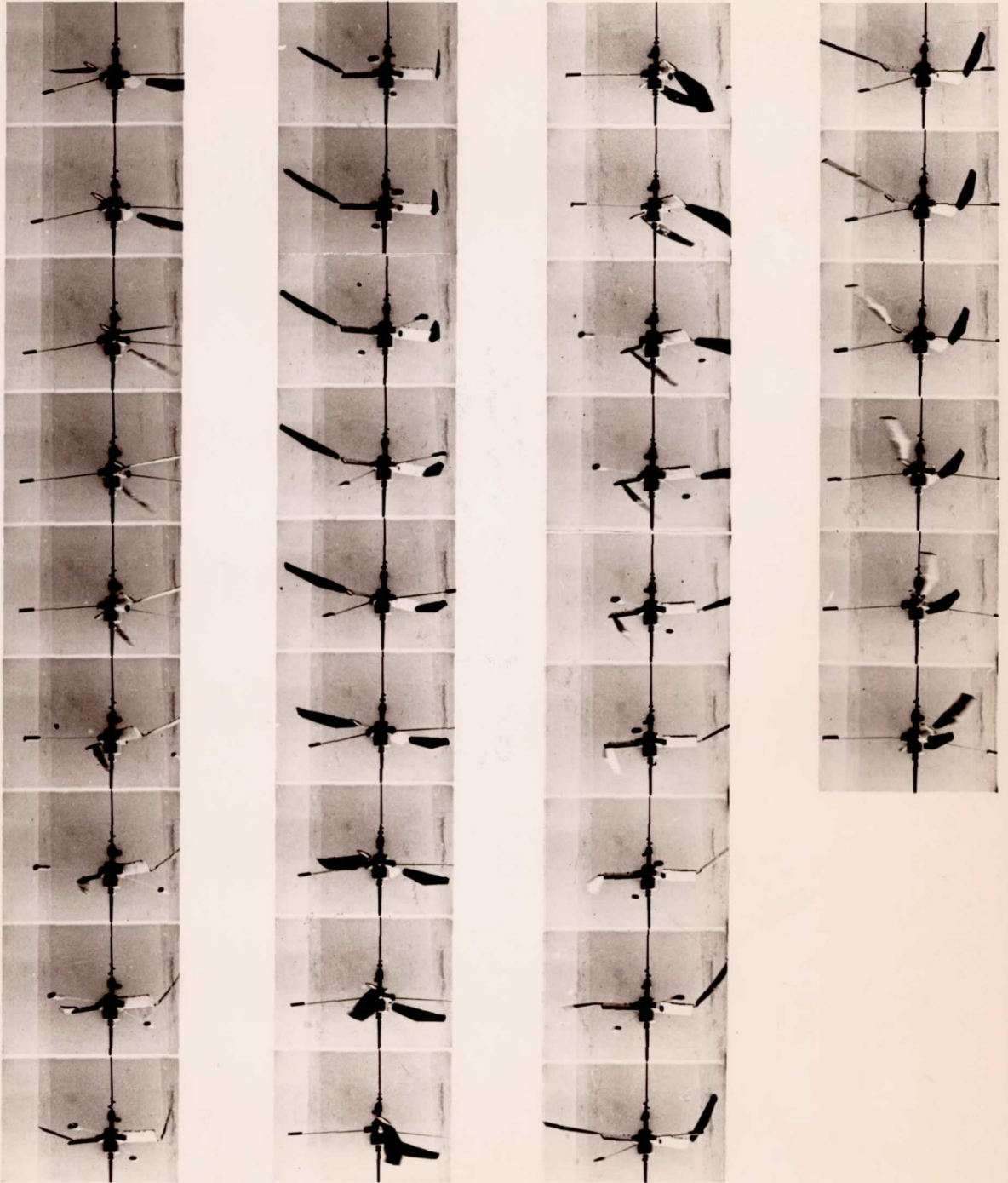
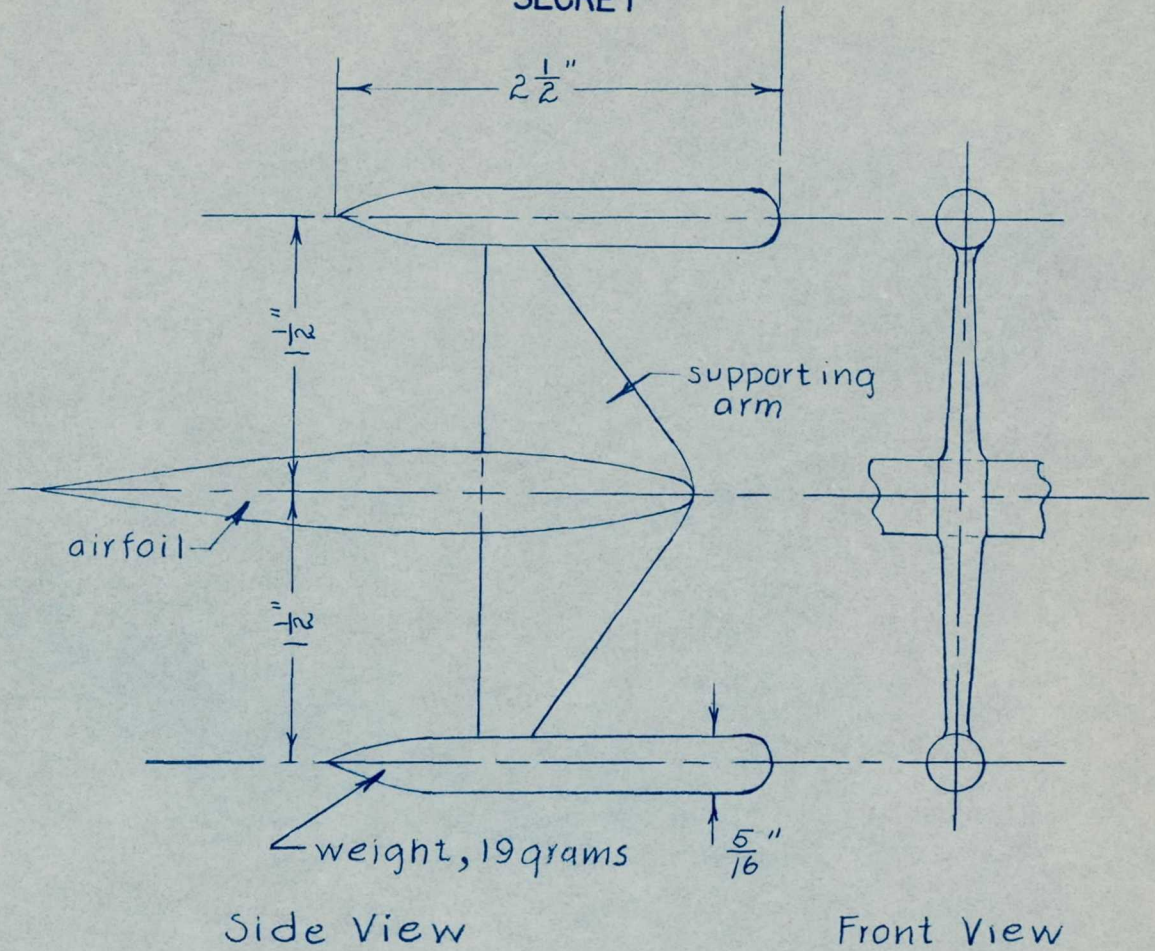


Figure 7.- Typical oscillatory motion of the blades after they extended beyond the cuffs. Camera speed 64 frames per second.

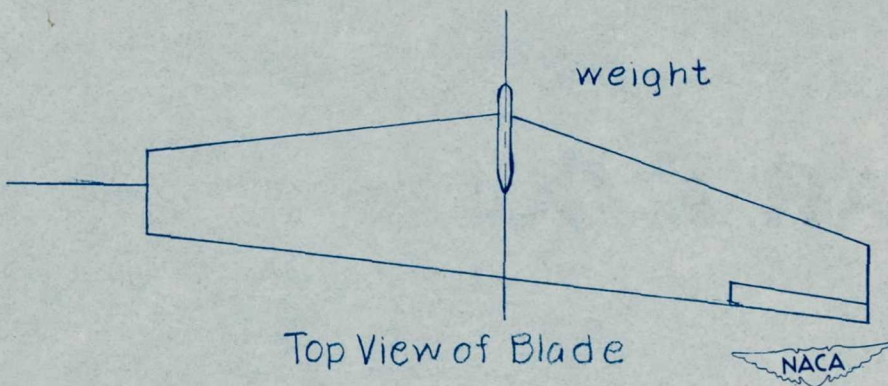
SECRET

SECRET

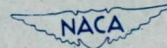


Side View

Front View



Top View of Blade



SECRET

Figure 8.- Compensating weights for blades of  $\frac{1}{4}$ -scale model of cargo-dropping device.

SECRET

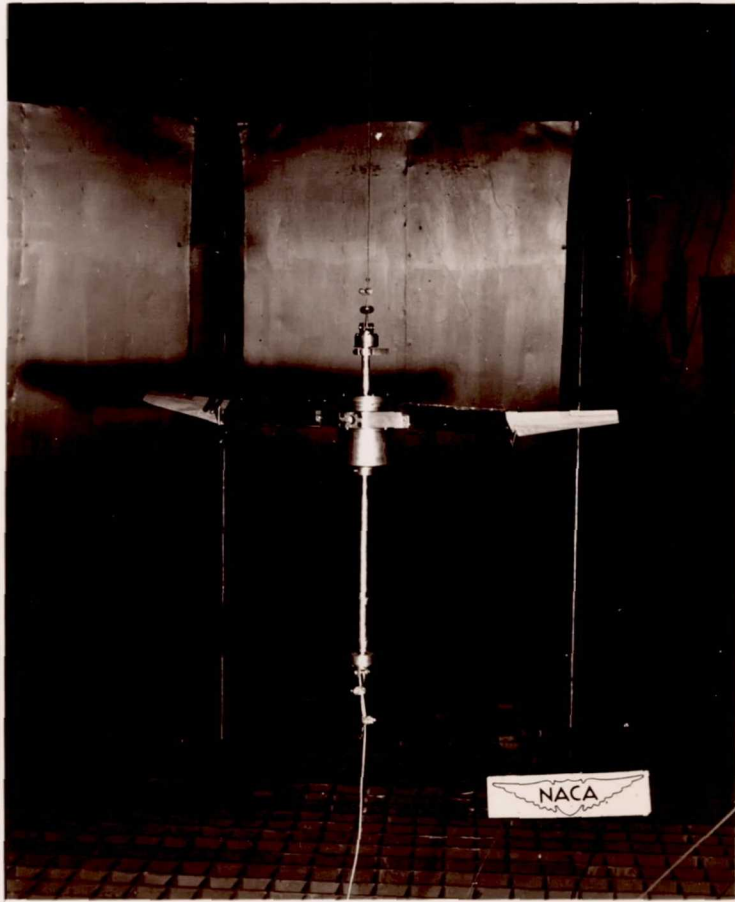


Figure 9.- Photograph of  $\frac{1}{4}$ -scale model of cargo-dropping device with cargo container removed; cuffs and compensating weights installed on the blades.

SECRET

SECRET

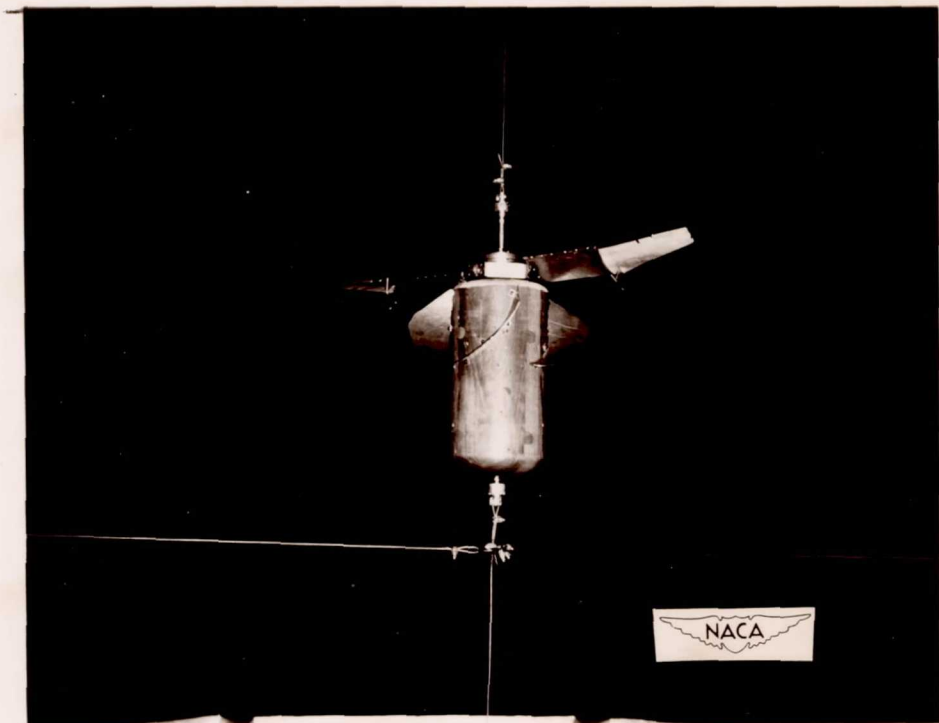


Figure 10.- Photograph of  $\frac{1}{4}$ -scale model of cargo-dropping device with cargo container installed; cuffs and compensating weights installed on the blades.

SECRET

SECRET

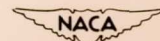


Figure 11.— Steady motion of the blades obtained with model when the inertia pitching moment of the blades was altered. Camera speed 64 frames per second. (Because of the limited view of the camera, only one blade can be seen in any given frame, and because of the relatively high rate of rotation, the blades appear as blurs in the fig.)

SECRET

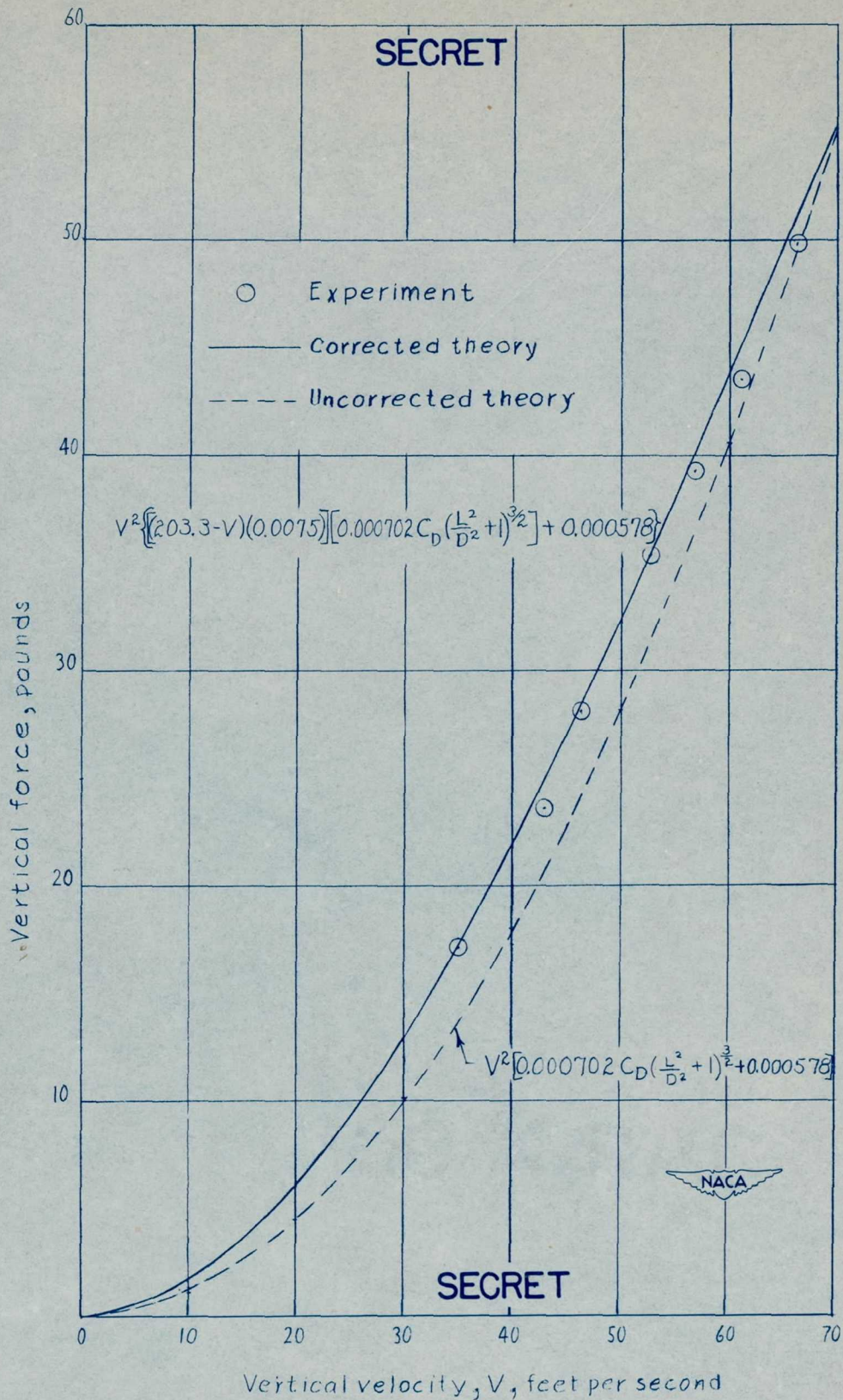
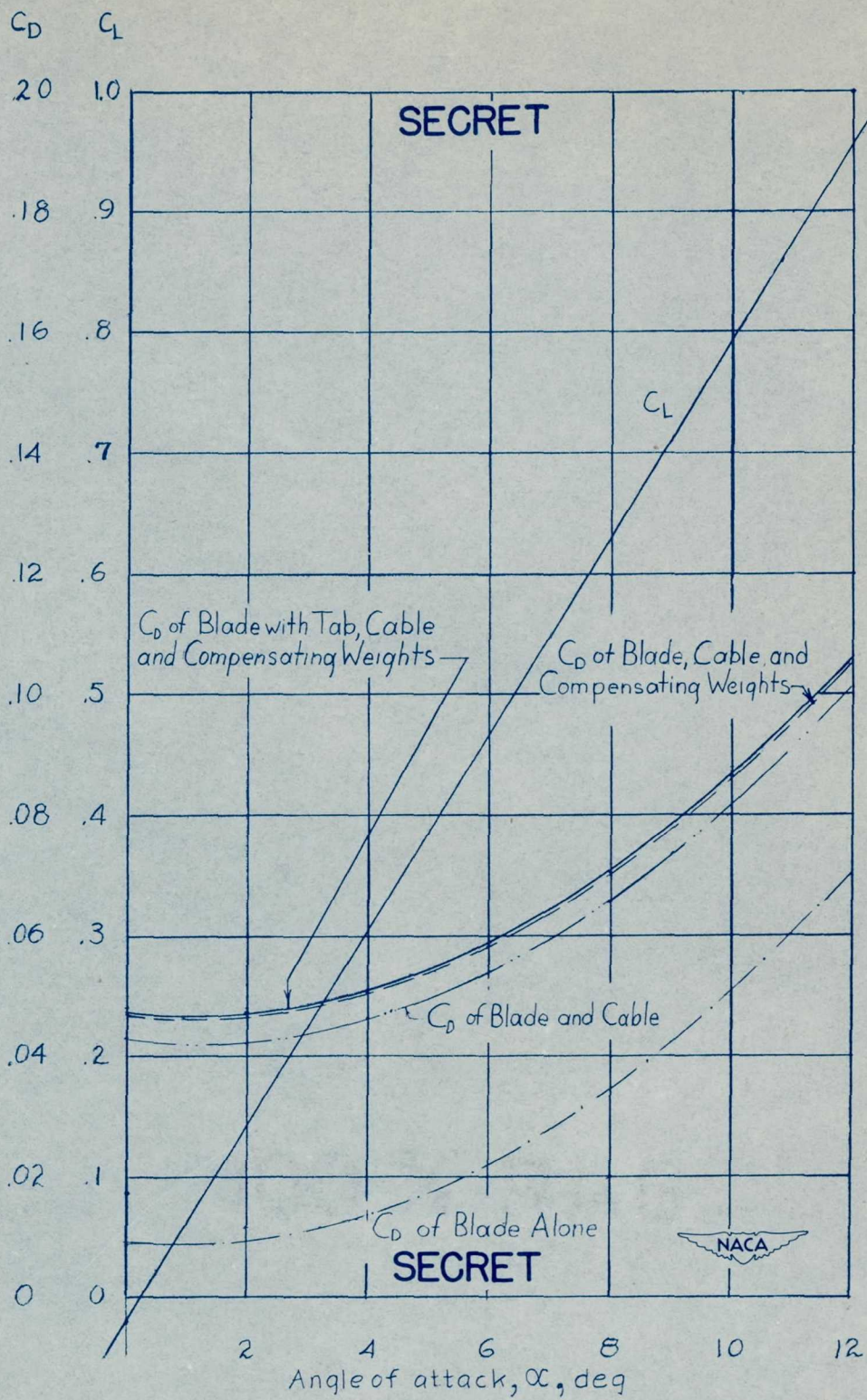
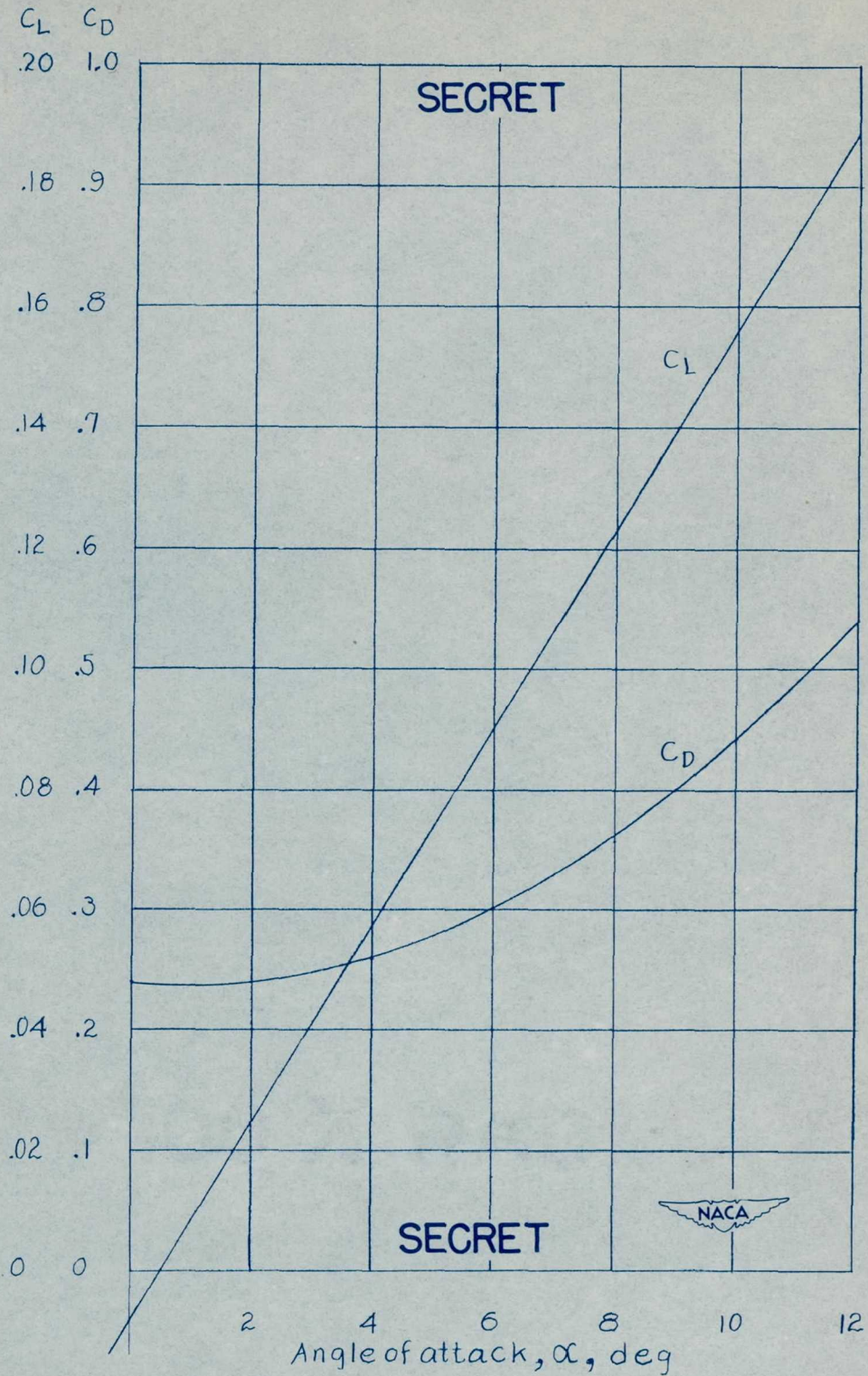


Figure 12.— Theoretical and experimental values of vertical force against vertical velocity for a  $\frac{1}{4}$ -scale model of the cargo-dropping device with two blades operating.

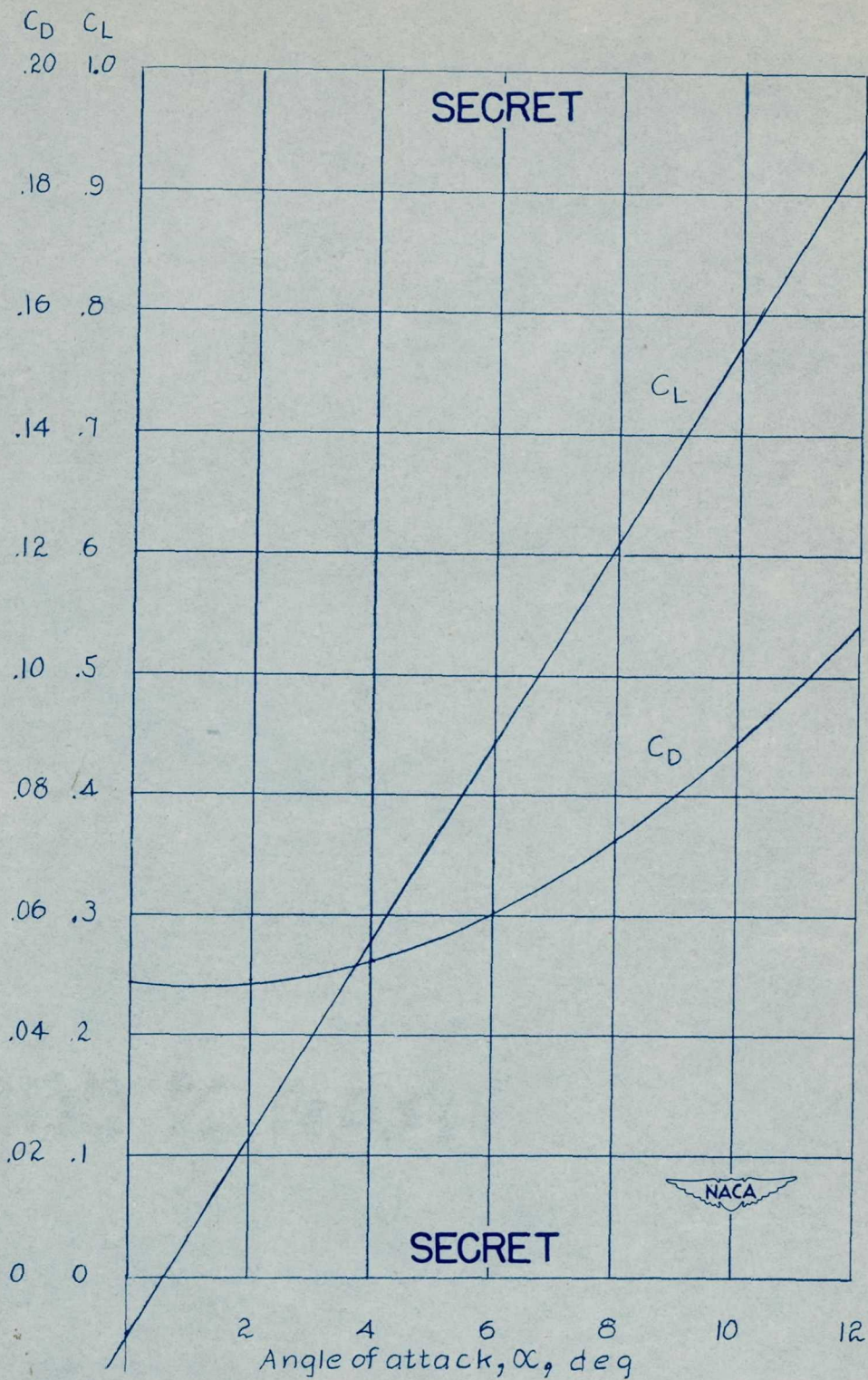


(a) With  $-5^\circ$  tab deflection.

Figure 13.- Estimated aerodynamic characteristics of NACA 65<sub>1</sub>-012 airfoil modified for aspect ratio 6, and drag of cable and compensating weights.

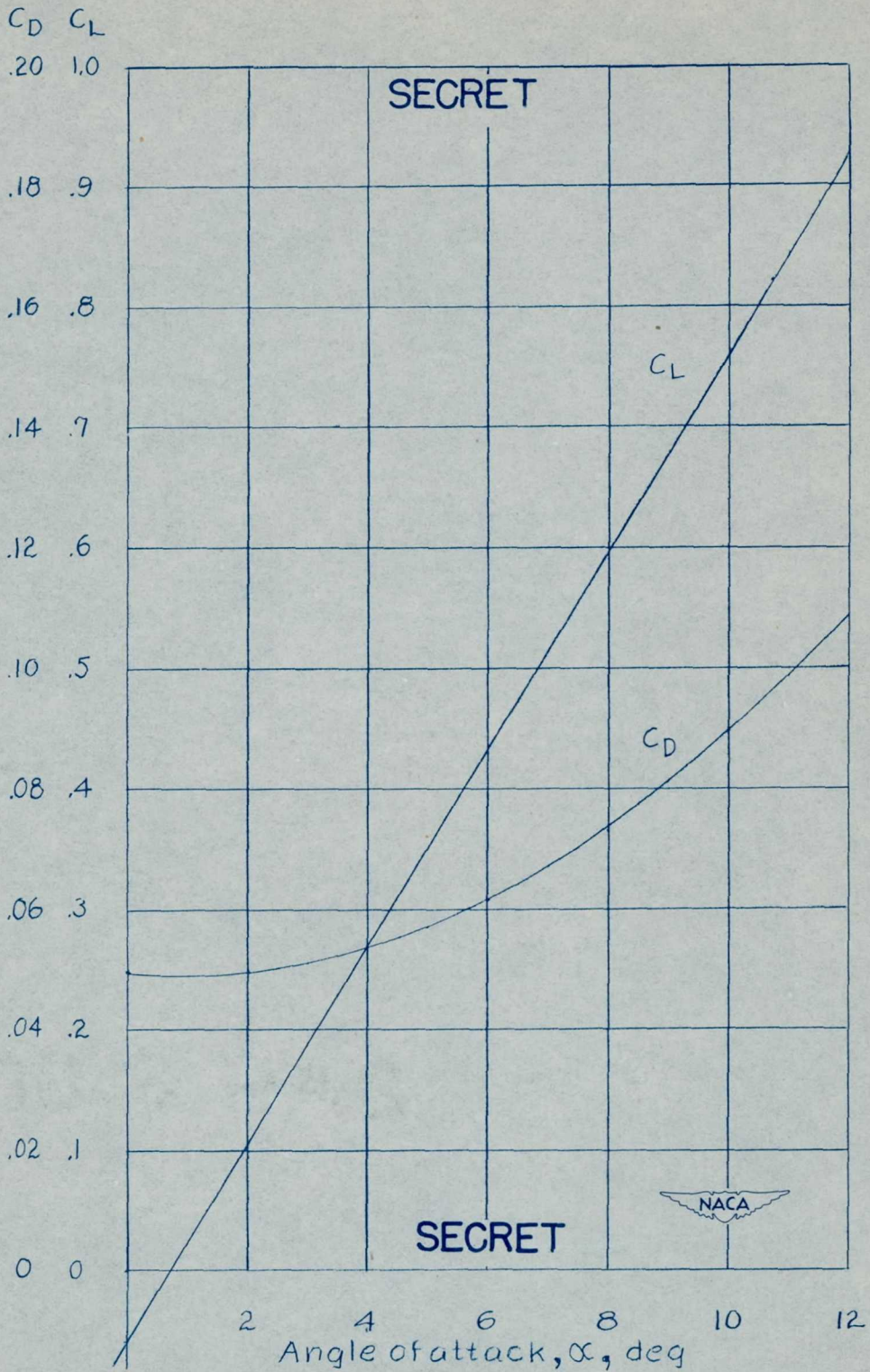


(b) With  $-10^\circ$  tab deflection.



(c) With  $-12^\circ$  tab deflection.

Figure 13.- Continued.



(d) With  $-15^\circ$  tab deflection.

$C_D$   $C_L$

.20 .10

.18 .9

.16 .8

.14 .7

.12 .6

.10 .5

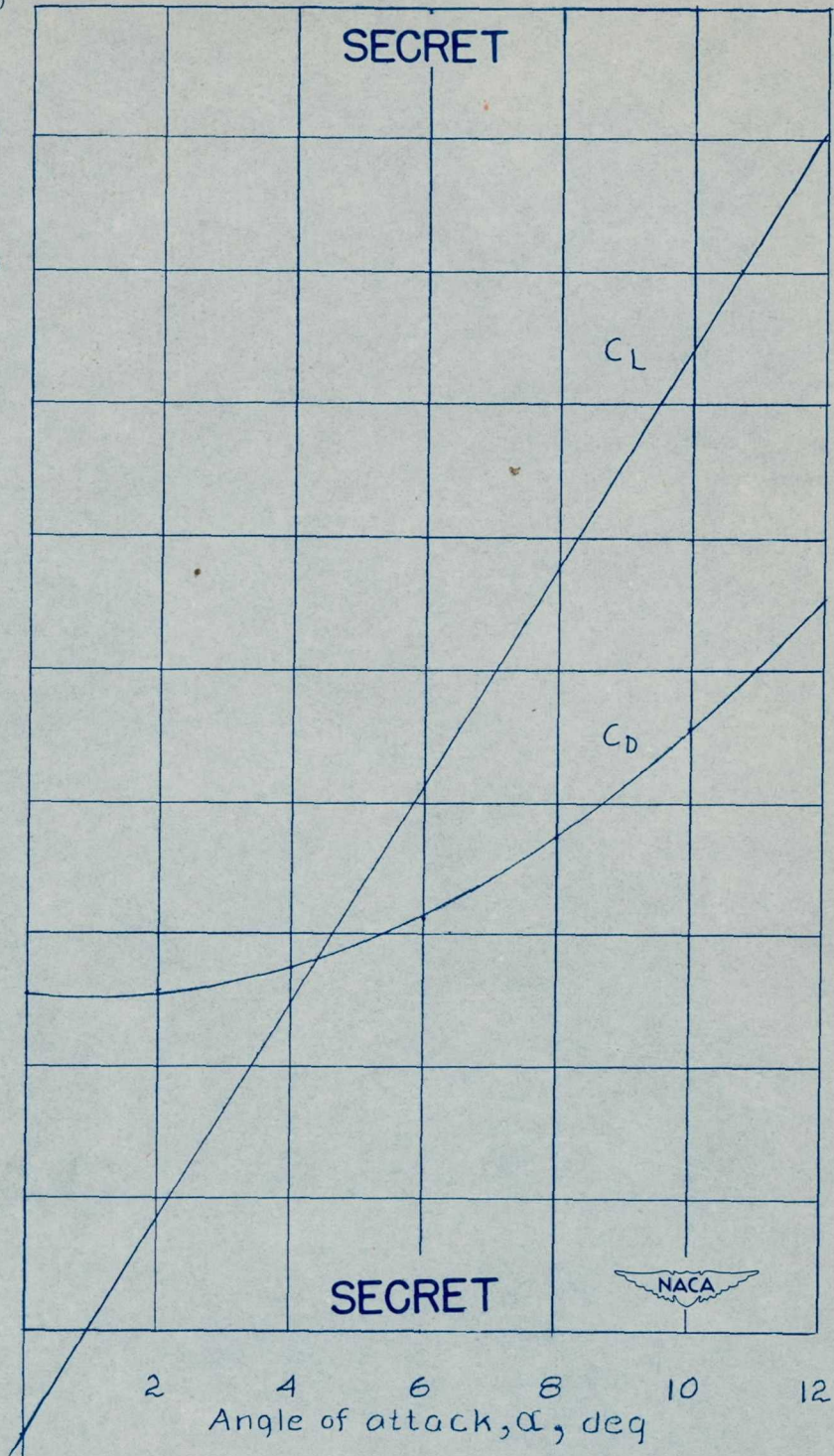
.08 .4

.06 .3

.04 .2

.02 .1

0 0



(e) With  $-20^\circ$  tab deflection.

Figure 13.- Concluded.

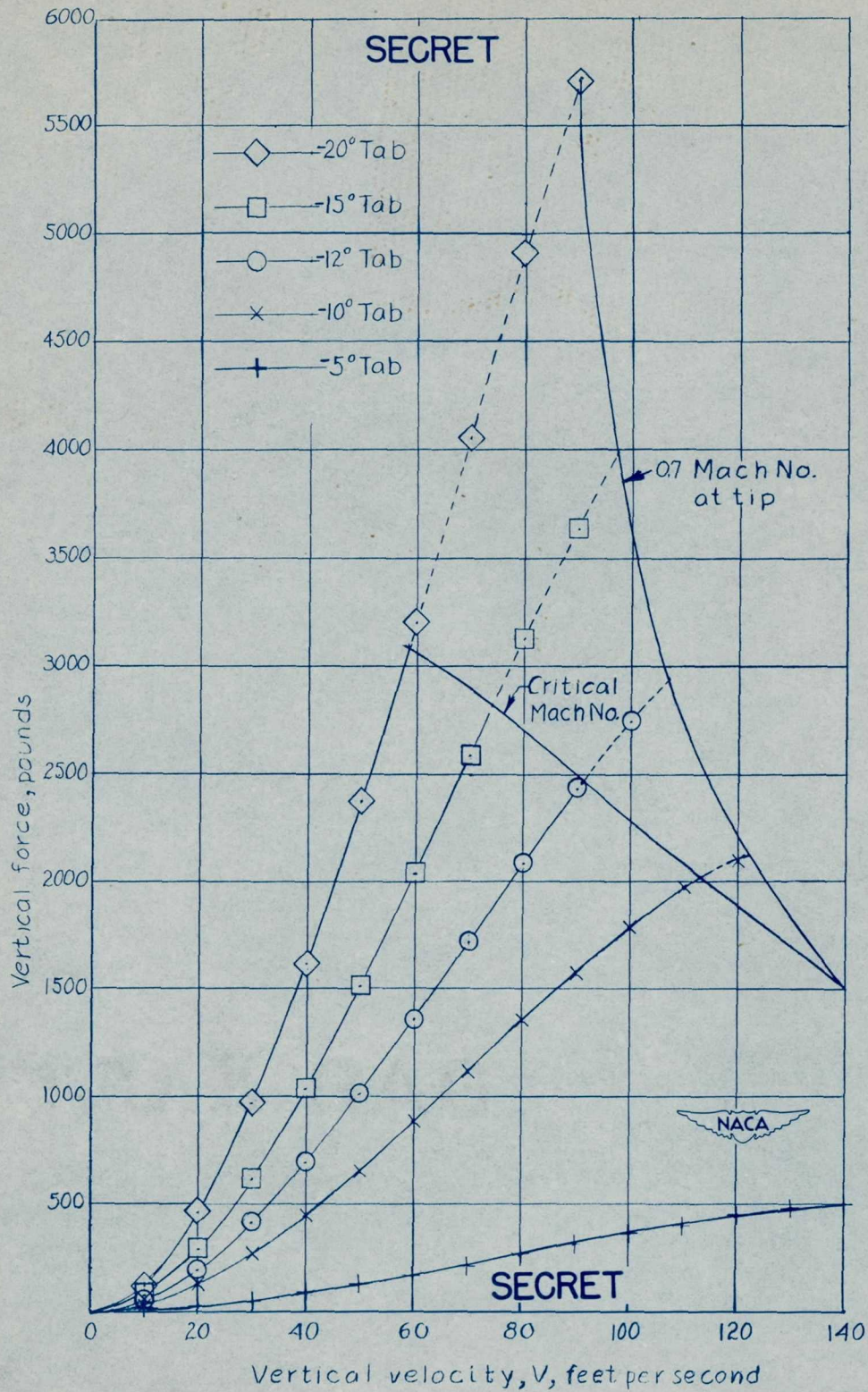


Figure 14.— Estimated performance of full-scale cargo-dropping device for various tab settings at sea level.

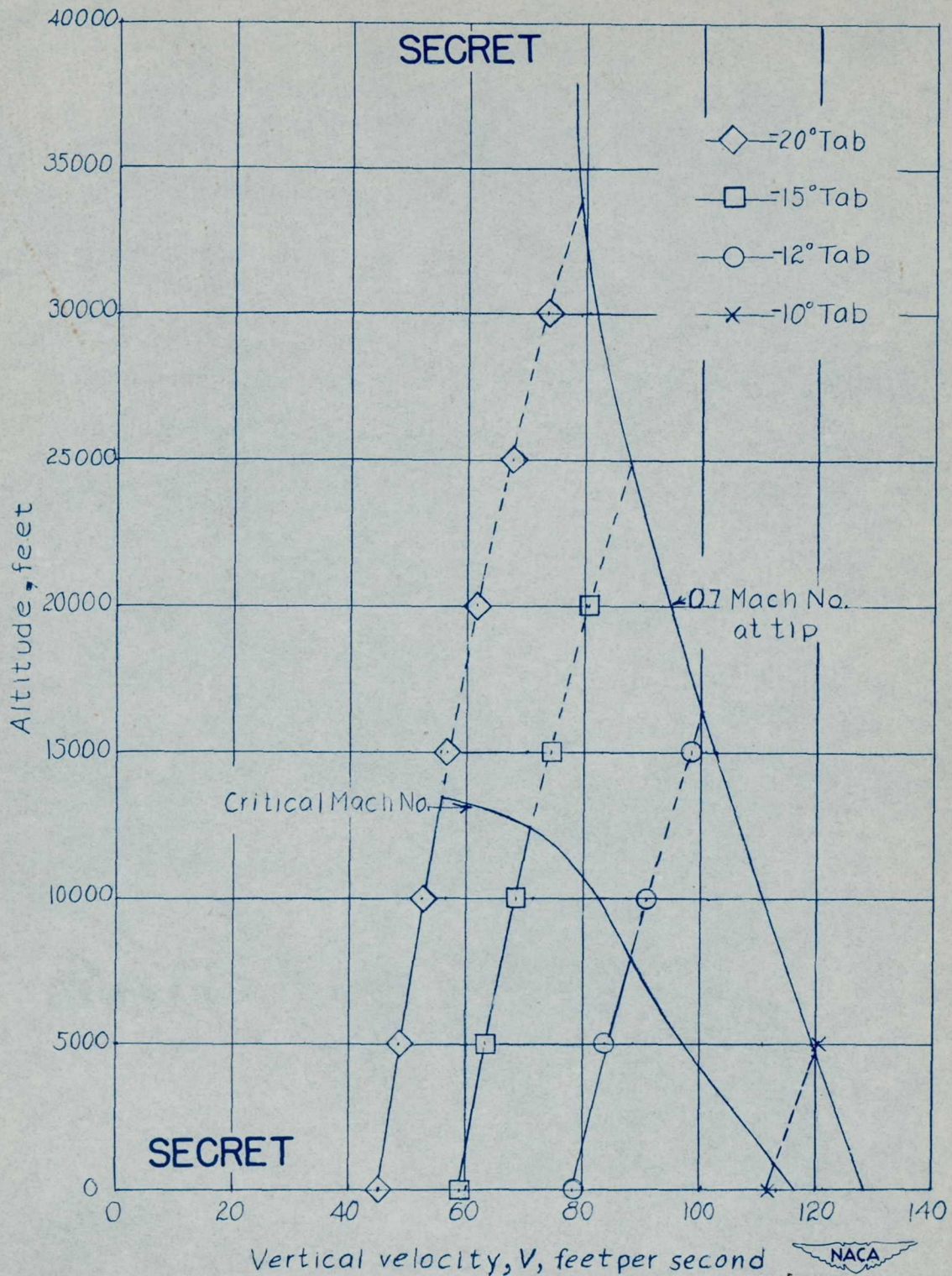


Figure 15.— Estimations of the variation of terminal velocity with altitude for cargo-dropping device with 2000-pound load for various tab settings.

SECRET

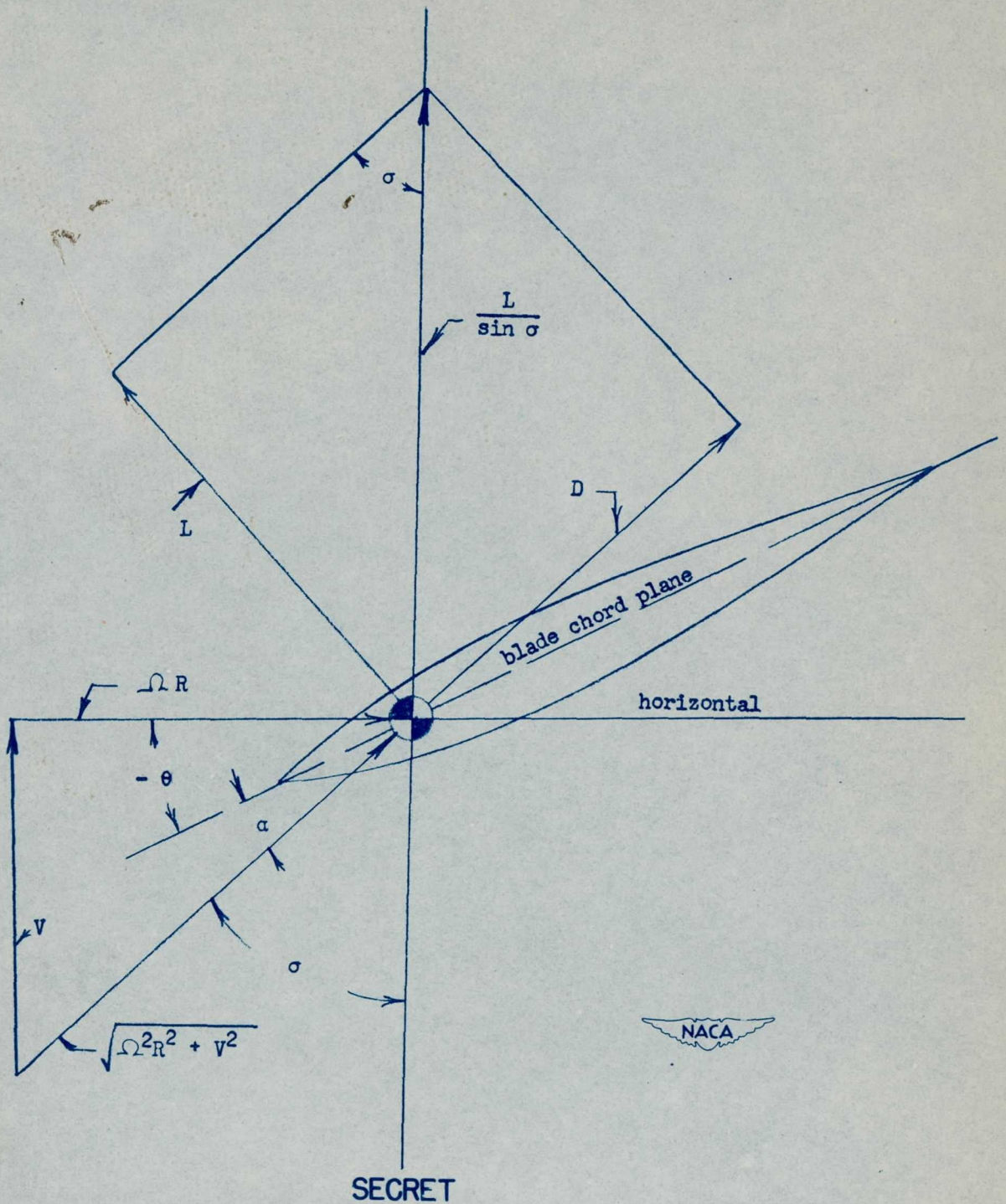


Figure 16.— Velocities and forces acting on rotating blade in equilibrium condition.



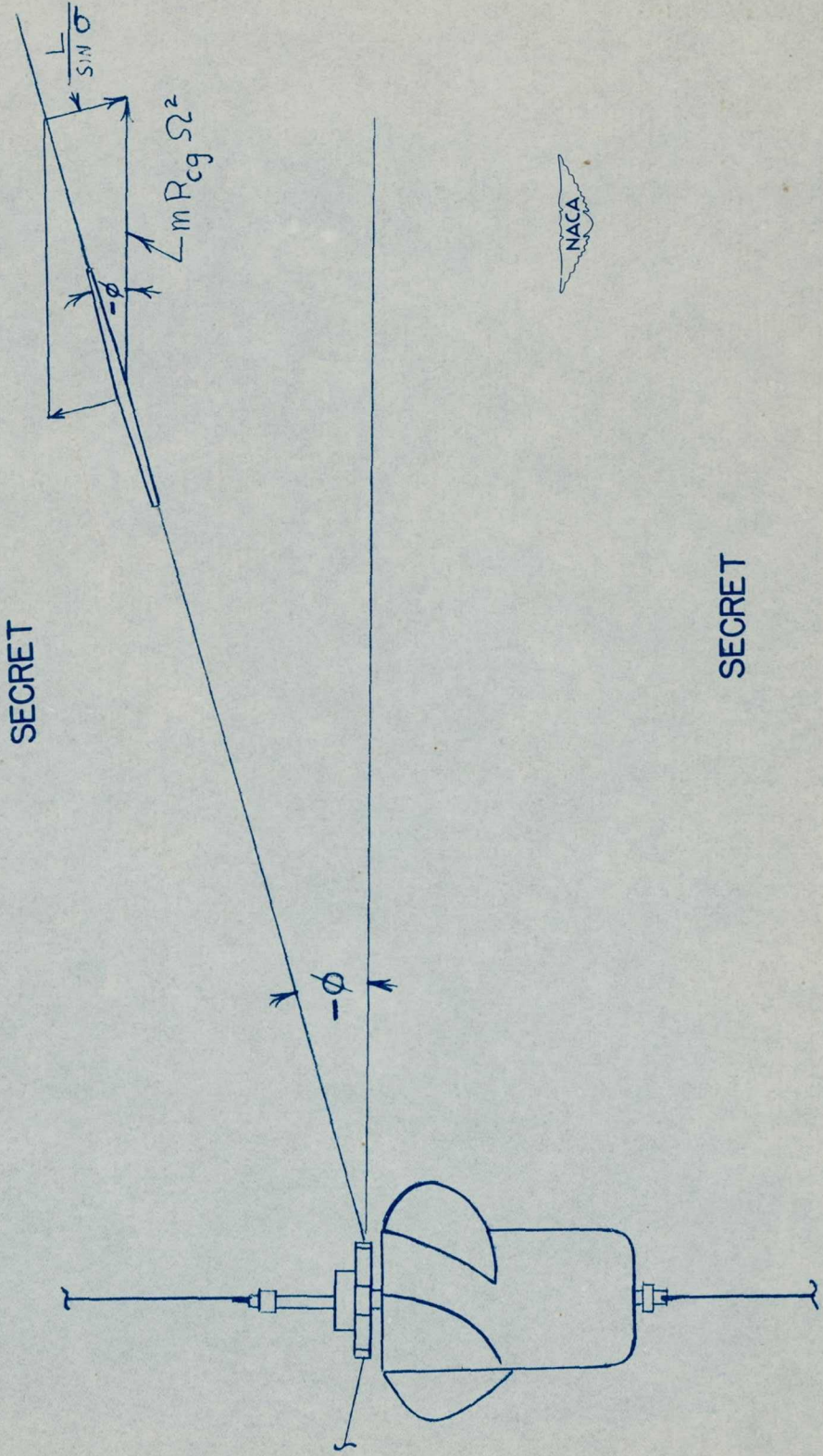


Figure 18.— Radial and vertical forces acting on blade and resultant spanwise blade attitude.

~~SECRET~~

INDEX

<u>Subject</u>	<u>Number</u>
Rotors - Experimental Studies	1.6.2
Rotors - Autorotating	1.6.2.2
Rotating-Wing Aircraft	1.7.3

ABSTRACT

The characteristics of a cargo-dropping device having extensible rotating blades as load-carrying surfaces have been studied in simulated vertical descent in the Langley 20-foot free-spinning tunnel.

The investigation included tests to determine the variation in vertical sinking speed with load. A study of the blade characteristics and of the test results indicated a method of dynamically balancing the blades to permit proper functioning of the device.

~~SECRET~~